Unveiling the Active Surface Sites in Heterogeneous Titanium-Based Silicalite Epoxidation Catalysts: Input of Silanol-Functionalized Polyoxotungstates as Soluble Analogues

Teng Zhang, Louis Mazaud, Lise-Marie Chamoreau, Céline Paris, Anna Proust, Geoffroy Guillemot

Unveiling the Active Surface Sites in Heterogeneous Titanium–Based Silicalite Epoxidation Catalysts: the Input of Silanol–Functionalized Polyoxotungstates as Soluble Analogues

*Teng Zhang,[†] Louis Mazaud,[†] Lise-Marie Chamoreau,[†] Céline Paris,[‡] Anna Proust[†] and Geoffroy Guillemot[†]**

[†] Sorbonne Université, CNRS, Institut Parisien de Chimie Moléculaire, IPCM, 4 place Jussieu, F-75005 Paris, France

[‡] Sorbonne Université, CNRS, De la Molécule aux Nano-objets: Réactivité, Interactions et Spectroscopies, MONARIS, 4 place Jussieu, F-75005 Paris, France

ABSTRACT.

We report on a site–isolated model for Ti(IV) by reacting $[Ti(^{i}PrO)_4]$ with the silanol–functionalized polyoxotungstates $[XW_9O_{34-x}(^{t}BuSiOH)_3]^{3-}$ (X= P, x=0, **1**; X= Sb, x=1, **2**) in tetrahydrofuran. The resulting titanium(IV) complexes $[XW_9O_{34-x}(^{t}BuSiO)_3Ti(O^{i}Pr)]^{3-}$ (X= P, **3**; X= Sb, **4**) were obtained in monomeric forms both in solution and in the solid state, as proved by diffusion NMR experiments and by X–ray crystallographic analysis. Anions **3** and **4** represent

relevant soluble models for heterogeneous titanium silicalite epoxidation catalysts. The POM scaffolds feature slight conformational differences that influence the chemical behavior of **3** and **4** as demonstrated by their reaction with H_2O. In the case of **3**, the hydrolysis reaction of the isopropoxide ligand is only little shifted towards the formation of a monomeric $[PW_9O_{34}(^t BuSiO)_3Ti(OH)]^{3-}$ (**5**) species [log K= –1.96], whereas **4** reacted readily with H_2O to form a μ-oxo bridged dimer $\{[SbW_9O_{33}(^t BuSiO)_3Ti]_2O\}^{6-}$ (**6**). The more confined the coordination site, the more hydrophobic the metal complex. By studying the reaction of **3** and **4** with hydrogen peroxide using NMR and Raman spectroscopies, we concluded that the reaction leads to the formation of a titanium-hydroperoxide Ti-(η^1–OOH) moiety, which is directly involved in the epoxidation of the allylic alcohol 3-methyl-2-buten-1-ol. The combined use of both spectroscopies also led to understanding that a shift of the acid-base equilibrium towards the formation of Ti(η^2-O_2) and H_3O^+ correlates with the partial hydrolysis of the phosphotungstate scaffold in **3**. In that case, the release of protons also catalyzed the oxirane opening of the in situ formed epoxide, leading to an increased selectivity for 1,2,3-butane-triol. In the case of the more stable $[SbW_9O_{33}(^t BuSiO)_3Ti(O^i Pr)]^{3-}$ (**4**), the evolution to Ti(η^2-O_2) peroxide was not detected by Raman spectroscopy and we performed reaction progress kinetic analysis by NMR monitoring the 3-methyl-2-buten-1-ol epoxidation in order to assess the efficiency and integrity of **4** as precatalyst.

KEYWORDS. Titanium, hydrogen peroxide, polyoxotungstate, silanol, site–isolated catalysts, epoxidation

1. INTRODUCTION

Substitution of Ti for Si in the framework of zeolites, first reported by Taramasso *et al.*,[1] resulted in the emergence of heterogeneous catalysts of practical use for the liquid–phase oxidation of various organic compounds at industrial scale.[2,3] The use of titanium, a first–row transition metal, and aqueous hydrogen peroxide, as terminal oxidant, make sense in view of the need to develop more sustainable oxidation processes.[4,5,6] The catalytic performances of microporous and crystalline titanium–silicalites (TS–1, a MFI zeolitic framework) are strictly associated to the structural peculiarities of the silica lattice.[7] First, the hydrophobic nature of the internal channel system favors the strong physisorption of the apolar substrates while preventing the hydrolysis of isolated titanium center. Conversely, the hydrophilicity of macroporous or amorphous Ti/SiO_2 more often results in leaching. Second, the metal ions are sufficiently held in the silica matrix, as a tripodal anchored species, to prevent conversion into inactive peroxide $Ti(\eta^2\text{-}O_2)$ species.[8,9] Indeed, the peracid-like mechanism is widely accepted for TS–1 catalyzed epoxidation, in which a hydroperoxo (Ti–OOH) rather than a peroxide species is involved. Modeling such a system at a molecular scale is rather difficult. One should mention the titanium-containing polyhedral oligomeric silsesquioxanes (POSS), probably the most relevant example, which enable the coordination of Ti in a tripodal siloxy coordination site.[10,11,12] Nevertheless the POSS ligands remain flexible enough to favor the expansion of the coordination shell and to easily promote the formation of dimers and also the generation of small embedded polyoxotitanate clusters $[TiOH]_4$ when in contact with water.[11] Accordingly the site–isolated model, as in heterogeneous systems, no longer applies.

A valuable molecular approach to catalytically active surface sites should fulfill the following criteria: the model system (i) should display a single isolated site with a geometrical and chemical local environment similar to the active site, (ii) should allow the successful

achievement of the same kind of transformations through a closely related chemical pathway. Moreover, a relevant molecular model should help to bring insights on the structure/activity relationships. The silanol–decorated polyoxotungstates (POTs) that are depicted in Figure 1 have proved to be capable of modeling surface vicinal silanols of dehydroxylated silica.[13] These organic hybrids of POTs may also best mimic the coordination environment of the tetrahedral defective open-lattice [(≡Si–O)$_3$Ti(OH)] sites[14,15] that are present in the microporous TS–1. First, the polyoxotungstic frameworks display a rigid and geometrically pre-organized set of silanol functionalities. Second, the *t*-butyl groups at the silicon atoms create a steric protection around the metal coordination site. The combination of these two factors prevents the formation of oligomers and allows the metal ion to fit in a well–defined isolated coordination site. We thus turned our attention to the synthesis of titanium complexes and their use as catalysts for the oxidation of alkenes by hydrogen peroxide. Indeed, most of the soluble titanium–silsesquioxane complexes so far reported were unsuitable for the use of aqueous solutions of hydrogen peroxide. Both irreversible hydrolysis of the SiO–Ti bonds and water inhibition of the active sites have been put forward to explain this lack of reactivity, which stands as a main drawback considering the attractive use of aqueous H_2O_2 solution as benign oxidant. Hence, different methods have been developed in order to immobilize titanium silsesquioxane complexes in a hydrophobic environment. Heterogeneous Ti-POSS systems have been prepared by grafting on a three-dimensional netted polysiloxane or by integrating into a SBA-15 supported polystyrene film by in situ copolymerization.[16,17] Encapsulation of Ti-POSS complexes in a dimethylsiloxane membrane has also been reported.[18] Despite the difficulty to control the three-dimensional structure of the polymer around the titanium complexes by these methods, it was established that

the hydrophobic network provided by the polymer enables the catalysts to display good H_2O_2 efficiency in alkene epoxidation and to be highly recyclable.

Polyoxometalates (POMs), which encompass the POTs family, are oxo clusters of early transition metals in their highest oxidation states (Mo^{VI}, W^{VI}, V^{V}). POMs are receiving much interest due to the great versatility of their molecular structures and properties. Usually considered as molecular analogues of metal oxides, POMs are robust, oxidatively and thermally. Among the numerous applications of POMs, catalysis surely occupies the first place: this concerns mainly acid catalysis due to the superacidity of heteropolyacids[19] and oxidation catalysis,[20] based on the intrinsic redox properties of POMs[21] or the incorporation of active transition metals.[22] The organic–inorganic hybrids **1** and **2** used in this study are built on two different types of trivacant Keggin heteropolyoxotungstates: $[PW_9O_{34}]^{9-}$ and $[SbW_9O_{33}]^{9-}$ (see Figure 1). The first one belongs to the A-type $[X(W_3O_{10})(W_2O_8)_3]^{n-}$ usually built around a tetrahedral *X* heteroatom such as P(+V) and the second one to a B-type $[Y(W_3O_{11})_3]^{9-}$ commonly obtained with pyramidal *Y* heteroatoms such as Sb(+III).[23] The organic functionalization of these species (by organosilanes in our case) is made possible by the enhanced nucleophilicity of the oxygen atoms which surround the vacancy.[24] For all the above-mentioned considerations, derivatives **1** and **2** represent good candidates for exploring oxidation catalysis by their corresponding titanium derivatives. Hereafter, we first focus on the description of the structural analogies with silica-supported titanium materials in order to validate our molecular model of heterogeneous systems. Secondly, we report our investigation on the catalytic activity of the titanium derivatives in the epoxidation of alkenes and allylic alcohols with H_2O_2. Our efforts have mainly focused on the identification of the active Ti-hydroperoxide intermediate and on

assessing the efficiency and integrity of the catalysts by performing reaction progress kinetic analysis by monitoring the oxidation reaction by NMR.

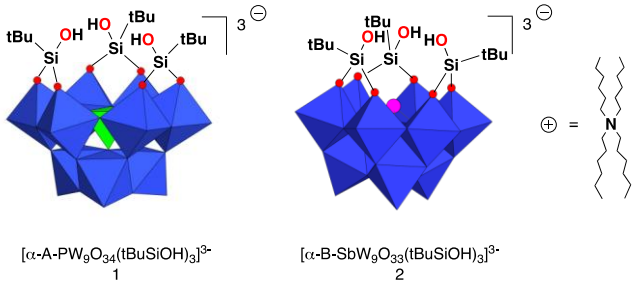

Figure 1. Anions 1 and 2 used in this study, prepared as tetrahexylammonium salts (THA). The polyoxotungstate frameworks are shown in polyhedral representation: tungsten in blue, phosphorus in green, antimony in magenta and oxygen atoms bordering the lacuna as red dots.

2. RESULTS AND DISCUSSION

2.1. The titanium complexes.

Synthesis. The synthesis of $[(\alpha\text{-A-PW}_9\text{O}_{34})(^t\text{BuSiOH})_3]^{3-}$ **(1)** and $[(\alpha\text{-B-SbW}_9\text{O}_{33})(^t\text{BuSiOH})_3]^{3-}$ **(2)** as tetrabutylammonium salts has been already discussed elsewhere.[25] We made use of quaternary ammonium cations with longer alkyl chains to enlarge the variety of organic solvents in which **1** and **2** could be soluble. When tetrahexylammonium (THA) salts were employed during the synthesis a good balance between increased solubility and ease of crystallization could be reached. As reported in our previous work, a preliminary heating of **THA-1** and **THA-2** under vacuum was needed to remove water molecules that remain physisorbed onto the POM and the SiOH functions (210°C at 10^{-3} mbar, 3h).[13] Then, a clean reaction of titanium tetra(isopropoxide) with the dehydrated silanol-functionalized POMs in tetrahydrofuran (THF) took place leading to the titanium derivatives **THA-3** and **THA-4** (eq 1) with the release of 3 equiv of 2-propanol, which can be monitored by NMR spectroscopy. NMR

analysis of collected **THA-4** revealed the presence of a by-product, in a very low amount (<5%), identified as a dimeric form, **THA-6**, which formation will be discussed below.

$$[XW_9O_{34-x}(^tBuSiOH)_3]^{3-} + Ti(O^iPr)_4 \rightarrow [XW_9O_{34-x}(^tBuSiO)_3Ti(O^iPr)]^{3-} + 3\ ^iPrOH \quad (1)$$

Structural characterization. Single crystals suitable for X-ray crystallographic analysis were obtained for **THA-3** and **THA-4**. As expected, both complexes are in monomeric forms (a complete data refinement for anion **4** is hampered by conformational disorder of the ammonium cations) (Figures 2 and 3). The geometric constraint imposed by the ligand forces the titanium center to adopt a quasi-regular tetrahedral geometry (mean value for the SiO–Ti–OSi angles = 110.5°), four oxygen atoms coordinating the metal center. It is worth emphasizing that the ≡Si–O and ≡SiO–Ti bond lengths in anion **3** and particularly those in anion **4** are very similar to those in TS-1 obtained by EXAFS studies.[26] Table 1 gathers the bond distances for ≡Si–O and ≡SiO–Ti and angle values for compounds **3** and **4** along with the corresponding values for TS-1 and two titanium-silsesquioxane complexes relevant to this work.

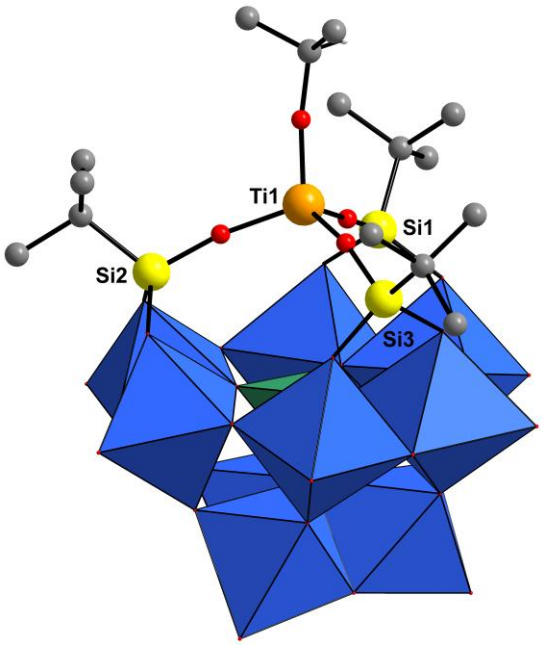

Figure 2. Crystal structure of anion 3.

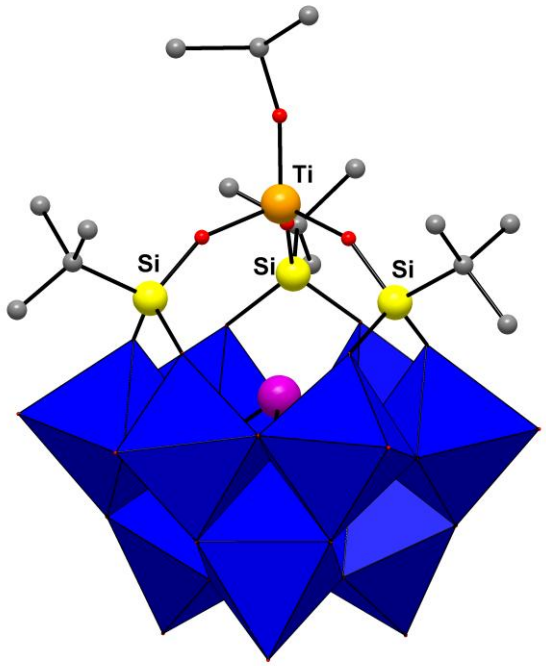

Figure 3. Model of the titanium derivative 4.

Table 1. Principal bond distances for ≡Si–O and ≡SiO–Ti and angle values.

		Si–O (Å) [a]	SiO–Ti (Å) [a]	Si–O–Ti (°) [a]	Ref.
1	Ti-silicalite (TS-1)	1.62	1.815	153.5	[26]
2	$[PW_9O_{34}(^tBuSiO)_3Ti(O^iPr)]^{3-}$, **3**	1.621(2)	1.804(3)	167.5	this study
3	$[SbW_9O_{33}(^tBuSiO)_{33}Ti(O^iPr)]^{3-}$, **4**	1.604 [b]	1.810 [b]	154.4 [b]	this study
4	$[(POSS)Ti(OSiMe_3)]$	1.625(6)	1.658(6)		[27]
5	$[(POSS)Ti(MeOH)(\mu\text{-}OMe)]_2$	1.619(8)	1.826(7)		[28]

[a] Mean value. [b] A complete refinement for 4 was hampered by disorder at the tetrahexyl ammonium cations.

Although a 3-fold symmetry is not crystallographically imposed, the NMR studies of **3** and **4** revealed the expected C_3 symmetry in solution. Moreover, the *t*-butyl groups at the silicon atoms function as NMR probe to confirm the introduction of the electron deficient $\{Ti–O^iPr\}^{3+}$ functionality as revealed by a slight low field shielding of the corresponding singlet (see experimental section). ^{31}P NMR chemical shift in anion **3** is little affected, thus indicating that the tungstophosphate core is retained. The crystal structures also confirm that the bulky *t*-butyl groups create a sterically protected single metal site (Figure S1). Noteworthy, the A-type $[PW_9O_{34}]^{9-}$ structure from **1** provides a lacuna which is slightly larger [*mean* diameter= 6.991 Å] than the lacuna provided by the B-type $[SbW_9O_{33}]^{9-}$ structure from **2** [*mean* d= 5.887 Å] which is reflected in the position of the silicon atoms and consequently the orientation of the *t*-butyl groups, pointing in a more axial fashion in **1** than in **2** (Figures 2, 3 and Figure S1). A second consequence is the more obtuse Si–O–Ti angles observed in anion **3** compared to those in **4**, 167.5° against 154.4° (Table 1). Considering again the electrophilic nature of the d^0–titanium center, it is reasonable to assume that the more obtuse the angle the more extended the stabilizing $O(p\pi) \rightarrow M(d\pi)$ bonding.[29] Overall, we can present anions **3** and **4** like accurate molecular models for the tripodal, open–lattice type titanium site depicted in siloxide and zeolite in which the metal atoms are tetra-coordinated with three ≡SiO– framework bonds and a terminal –OH group.

Reactivity towards water. Hydrophobicity is a key point governing the efficiency of the titanium systems in liquid–phase oxidation reactions by TS–1 compared to amorphous Ti-SiO_2 systems. NMR monitoring of gradual addition of water to the solutions of **3** or **4** in dry acetonitrile–d_3 showed the progressive release of 2–propanol as a result of the protonolysis of the remaining isopropoxide. Whereas the alcohol release was rather unfavorable in the case of **3**

[log(K)= –1.96], compound **4** reacted readily with water. DOSY NMR spectroscopy provided clues to help in the identification of the hydrolysis products, monomeric Ti–hydroxide *vs*. dimeric Ti–hydroxide or oxide. Compound **3** and its product of hydrolysis, **5**, displayed the same diffusion coefficients and therefore **5** can be defined as a monomeric titanium-hydroxyde $[PW_9O_{34}(^tBuSiO)_3Ti(OH)]^{3-}$ species (eq 2).

$$[PW_9O_{34}(^tBuSiO)_3Ti(O^iPr)]^{3-}\ (\mathbf{3}) + H_2O \leftrightarrows [PW_9O_{34}(^tBuSiO)_3Ti(OH)]^{3-}\ (\mathbf{5}) + {}^iPrOH \quad (2)$$

In contrast, the diffusion coefficient of **6,** the product of hydrolysis of compound **4**, appeared markedly smaller (Table S2 and Figure S2). The collected data strongly support the formation of a μ-oxo bridged dimer $\{[SbW_9O_{33}(^tBuSiO)_3Ti]_2O\}^{6-}$ according to eq 3. Formation of such dimers has been reported for heterogeneous systems[30] as well as for other Keggin type polyoxometalates[31,32,33] incorporating titanium centers.

$$2\ [SbW_9O_{33}(^tBuSiO)_3Ti(O^iPr)]^{3-}\ (\mathbf{4}) + H_2O \leftrightarrows \{[SbW_9O_{33}(^tBuSiO)_3Ti]_2O\}^{6-}\ (\mathbf{6}) + 2\ {}^iPrOH \quad (3)$$

The hydrolysis product **THA-6** was also clearly identified as the by-product in the synthesis of **THA-4**. Since we rigorously worked under anhydrous conditions, we should mention that anion **4**, as a metal alkoxide, could undergo a non-hydrolytic condensation (referred to as alcohol dehydration) to give a μ-oxo bridged binuclear species through the elimination of diisopropylether or a propene / 2-propanol mixture (Scheme S1).[30,34] Compound **6** can be easily isolated and elemental analytical and NMR data clearly indicate that no bridging isopropoxide or isopropanol ligands are present. Indeed, the titanium ion in **6** remains four-coordinate, and the formation of the dimer is made possible because of the smaller bulk provided by the *t*-butyl groups in **2** (Figure S1 and Scheme S1) [Note: this assignment was supported by a preliminary

X-ray analysis, which revealed the dimeric structure]. The system described herein contrasts with the reported titanium silsesquioxane [(*c*-hexyl)$_7$Si$_4$O$_9$(SiO)$_3$Ti(OR)] series where titanium(IV) can accommodate coordination numbers ranging from 4 in the monomeric form (R= Me$_3$Si)[27] to a 5 and 6 in alkoxy-bridged dimers (R= ^{i}Pr or Me).[28] It is worth noting that the formation of the μ-oxo bridge does not prevent the use of **THA-4** as precatalyst since addition of H_2O_2 or an excess of alcohol shifts back the equilibrium towards the formation of the monomeric titanium-alkoxide (*vide infra*, 'NMR spectroscopy' section).[30,35,36] Overall these results tend to indicate that the formation of Ti–OH bond is not favorable and instead, the formation of a Ti–O–Ti bond is more likely the primarily driving force of hydrolysis. We aim at using and developing a system in which the metal center would fit in a confined and rigid coordination site with possibly a hydrophobic environment. The titanium complexes reported herein meet fairly well these requirements.

2.2. Applicability for the catalytic olefin epoxidation with H_2O_2.

When dealing with the use of POMs as catalysts in oxidation reactions with hydrogen peroxide, one should first bear in mind the solvolytic instability of most $[XW_{12}O_{40}]^{n-}$ Keggin type structures in aqueous hydrogen peroxide solutions.[37,38] Degradation of the oxotungstate core proceeds through the release of $\{WO_2\}^{2+}$ species which can further react with H_2O_2 to form Mimoun–[39] or Venturello–like species,[40] both active in olefin epoxidation.[41,42,43] In the case of hybrids of POMs, both base- and acid-catalyzed hydrolysis may lead to the release of silanol arms and the generation of *cis*–W(=O)$_2$ units (Scheme S2).[44] The latter have been proven to react with hydrogen peroxide to afford *cis*-WO(η^2-O$_2$) species, which explains the remarkable catalytic activities of the lacunary $[\gamma\text{-}SiW_{10}O_{34}(H_2O)_2]^{4-}$ and $[CoW_{11}O_{39}]^{9-}$, both related to the

Keggin structures.[45,46] The involvement of lacunary species in POM-catalyzed oxidation reactions with hydrogen peroxide is thus most commonly accepted. Some rare examples of non–lacunary heteropolyoxometalate stable towards H_2O_2 have been reported, among which we can mention the titanium–substituted heteropolyoxotungstates reported independently by the groups of Kholdeeva,[47,48] Mizuno,[49,50] and Nomiya.[33,51] Because of the question of solution stability, a particular attention must be paid to the origin of the catalytic activity observed for **3** and **4**, which means Ti–centered or W–centered. To this purpose we first probed the stability of the precursors **THA–1** and **THA–2** in the standard conditions that we use (1 mol% vs olefin) for the oxidation of 3–methyl–2–buten–1–ol (0.26 M), our substrate of reference, with a 30%wt aqueous solution of hydrogen peroxide ($[H_2O_2]_i$ = 0.26 M) in acetonitrile. While they are not expected to be active, monitoring the reaction by NMR clearly indicated the *undesired* conversion of the unsaturated alcohol to epoxide over time when using **THA-1** (Figure S3). ^{31}P NMR analysis of the catalytic mixture revealed the presence of new lines at -12.3 ppm, -12.6 ppm and -14.5 ppm of small relative intensities compared to the main line at -16.9 ppm (**1)**. These revealed the solvolytic instability of **1** and the formation of small quantities of partially hydrolyzed derivatives (Scheme S2).[52] Conversely, anion **2** showed a much greater robustness to hydrolysis: at room temperature, no significant conversion to epoxide was observed for the first four hours, and then, conversion started only very smoothly (Figure S3). Over these first four hours, the H_2O_2 concentration did not decrease significantly, showing that the precursor **THA-2** also did not catalyze the decomposition of hydrogen peroxide. Hence, in our conditions, $[SbW_9O_{33}(^t BuSiOH)_3]^{3-}$ scaffold represent the best precursor and we thus focused our attention on the catalytic behavior of its titanium derivative (**4**).

Catalytic Olefin Epoxidation. Attempts to oxidize unfunctionalized olefins, even an electron–rich olefin such as 2–methyl–2–pentene, were unsuccessful, conversions remaining insignificant (Table 2). Concerning allylic alcohols, conversions were observed when nucleophilic olefins were employed, such as 3–methyl–2–buten–1–ol, whereas oxidation was almost unsuccessful in the case of 2–propen–1–ol. Monitoring the olefin conversion over time clearly indicated that the epoxidation starts readily and can reasonably be attributed to a titanium–centered oxidation process (Figure 4).

Table 2. Epoxidation of Olefins Catalyzed by $(THA)_3[SbW_9O_{33}(^tBuSiO)_3Ti(O^iPr)]$, THA-4, with a 30wt% aqueous solution of H_2O_2 [a]

			Selectivity (%) [c]			r_0
Entry	Olefins	Conv [b] (%)	Epox	Triol	Aldehyde	(mM min^{-1})
1	2-methyl-2-pentene	<5	*n.a.* [d]	-	-	
2	2-propen-1-ol	<5	*n.a.* [d]			
3	3-methyl-2-buten-1-ol [e]	57	80	8.2	9.3	1.43
4	*trans*-2-penten-1-ol	75.5	63.5	28.7	7.7	

[a] All reactions were carried out in acetonitrile at room temperature (20°C) with [catalyst]= 2.6 mM, $[olefin]_0=[H_2O_2]_0$= 0.26 M. [b] Conversion is based on NMR analysis after 21 h of reaction. [c] Undefined side products are not listed. [d] The conversion is too low to ascertain the selectivity in epoxide. [e] When THA-3 was used as pre-catalyst initial rate measurement gave: r_0= 0.38 mM min^{-1}.

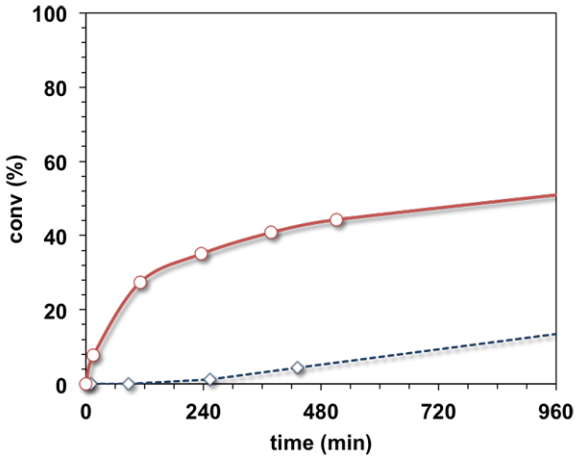

Figure 4. Plot of 3–methyl–2–buten–1–ol conversion as a function of time in the oxidation by H_2O_2 in CD_3CN at room temperature, catalyzed by 1 mol % $(THA)_3[SbW_9O_{33}(^tBuSiOH)_3]$, THA-2 (◇, dashed line), and its titanium derivative $(THA)_3[SbW_9O_{33}(^tBuSiO)_3Ti(O^iPr)]$, THA-4 (○) ; $[olefin]_0=[H_2O_2]_0= 0.26$ M.

From these observations we can assume that: (i) the species formed from the interaction of titanium with hydrogen peroxide is not very reactive, i.e. the proximal oxygen atom to the titanium center is not electrophilic enough, (ii) olefin binding to the oxophilic titanium center (through the alcohol function) is required to get an efficient conversion and, (iii) the mechanism proceeds through a peroxidic pathway[53,54] in which the olefins, as nucleophiles, react with the metal-bound electrophilic oxygen in a back side approach.[55,56] The second point is also corroborated by the oxidation of geraniol (*trans*–3,7–dimethyl–2,6–octadien–1–ol), which affords a selectivity of 95:5 for the 2,3–epoxy geraniol (Scheme 1).

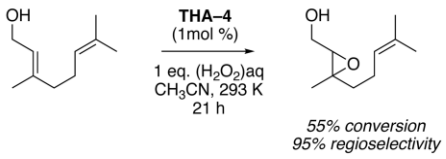

Scheme 1. Epoxidation of geraniol with H_2O_2 catalyzed by THA-4.

In the case of *trans*–2–penten–1–ol a higher conversion was obtained, most probably thanks to the decrease of the bulkiness at the active olefinic group. However, the selectivity of the corresponding triol (1,2,3-pentanetriol) was also higher (28.7%). Triol originates from a conventional two–step dihydroxylation: epoxide formation followed by its hydrolysis. Its formation has been often explained by a slight acidic behavior of a titanium-hydroperoxide species that is postulated to form *in situ* and which promotes an acid–catalyzed oxirane ring opening.[57] It is however noteworthy that the higher triol selectivity observed in the case of *trans*–2–penten–1–ol compared to 3–methyl–2–buten–1–ol tends to favor oxirane opening through a nucleophilic substitution pathway in which a titanium hydroxide as intermediate, [Ti]–OH, could be also involved. Finally, beside the epoxide formation, oxidation of the alcohol functionality leading to the formation of α,β-unsaturated aldehyde occurs to a negligible extent (probably also through a heterolytic mechanism). This dehydrogenation is expected to prevail when the electrophilic character of the proximal oxygen atom diminishes.[58]

2.3. Evidence for a [Ti]–hydroperoxide as active species.

It is worth noticing that in aqueous solutions of hydrogen peroxide, titanium salts are known to evolve into the more stable Ti(η^2-O_2) side-on peroxide species. Several Ti-peroxo complexes have been structurally characterized by X-ray diffraction; however, when isolated they usually proved to be not active for oxygen atom transfer to olefins (contrary to their tungsten or molybdenum analogues).[59,60] A Ti_2–μ– η^2: η^2-peroxo core embedded in a [γ-$PW_{10}O_{36}$]$^{7-}$ phosphotungstate framework represents the only example of Ti-peroxide reported to be active for

oxidation.[50] In the heterogeneous TS–1/H_2O_2/H_2O system, the generation of Ti(η^2-O_2) species has been supported by Raman spectroscopy analysis. The appearance of a strong and sharp mode at 618 cm^{-1} has been ascribed to a vibration mode of the Ti-peroxide complex by comparison with the structurally characterized $(NH_4)_3[TiF_5O_2]$ model compound.[61,62] This very characteristic band is resonance–enhanced when tuning the exciting laser source within the specific LMCT transition ($Ti^{4+} \leftarrow O_2^{2-}$, centered at 385 nm in TS-1). The combined use of XANES/EXAFS spectroscopy with common techniques (UV-vis, Raman, IR) and quantum chemical methodologies led to agree on the following points: first, the exothermic formation of Ti–(OOH) is consistent with both η^1 or η^2 bonding modes;[9] secondly, in the presence of water an acid–base equilibrium results in the formation of the side-on Ti(η^2-O_2) peroxide species and H_3O^+, thus increasing the acidity of the TS–1/H_2O_2/H_2O system.[63] Importantly, the titanium hydroperoxo species has been described as colorless while the titanium peroxo species was yellow (λ_{max} = 385 nm).[61,63] Despite these studies, and mostly because of the lack of relevant homogeneous models, the detailed structure of the active intermediate is still a matter of debate.[64,65] We thus decided to follow by several spectroscopic analysis the evolution of **3** and **4**, which represent relevant homogeneous models, when in contact with H_2O_2 and 3-methyl-2-buten-1-ol. Some of the results are summarized in scheme 2 and discussed below.

NMR spectroscopy. In order to gain a deeper understanding of the nature of the active species involved in the catalytic reaction, we first followed by NMR the effect of the addition of H_2O_2 (as a 30 wt% aqueous solution) on 5.2 mM solutions of **3** and **4** in deuterated acetonitrile. In the case of **3**, the addition of 3 eq of H_2O_2 led to almost complete conversion into a single new 3 fold–symmetric species, **7**, along with the release of 1 eq of 2–propanol. By adding 4 eq of 3-methyl-2-buten-1-ol to this solution, the progressive formation of the corresponding epoxide was

observed. After consumption of the hydrogen peroxide, the complex **7** disappeared in favor of a mixture of anions **3**, $[PW_9O_{34}(^tBuSiO)_3Ti(O^iPr)]^{3-}$, and **5** $[PW_9O_{34}(^tBuSiO)_3Ti(OH)]^{3-}$ (Figure S4). The same trend was observed when using anion **4**: upon addition of H_2O_2, a new species formed, **8**, epoxidation occurred, and after complete consumption of H_2O_2 anion **8** disappeared in favor of **6**, which is formed preferentially in these conditions (Figure 5 and Figure S5). These results clearly suggest the formal substitution of the incoming H_2O_2 molecule for isopropoxide ligand as a first step, thus leading to the formation of the Ti–hydroperoxide species (either η^1 or η^2–bonded) $[PW_9O_{34}(^tBuSiO)_3Ti(OOH)]^{3-}$ (**7**) and $[SbW_9O_{33}(^tBuSiO)_3Ti(OOH)]^{3-}$ (**8**).[66]

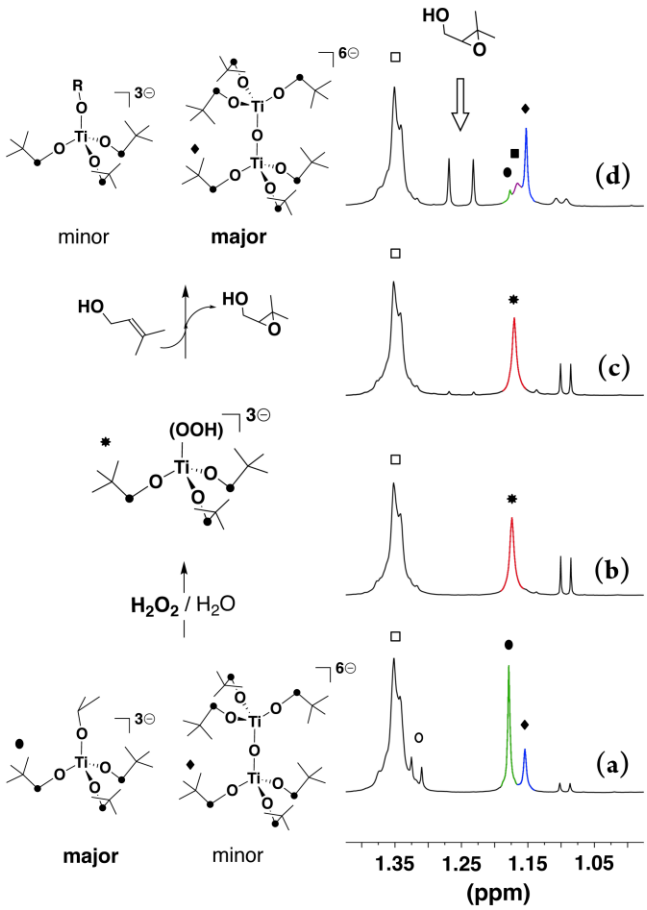

Figure 5. ^1H NMR monitoring of the evolution of a 5.2 mM solution of $(THA)_3[SbW_9O_{33}(^tBuSiO)_3Ti(O^iPr)]$, THA-4, in acetonitrile-d_3: (a) THA-4 (●, major) and its

related dimer, THA-6 (♦, minor); peaks reported by a □ mark belong to the THA cations; (b) formation of THA-8 after addition of aqueous H_2O_2 (30wt%) to (a) ; (c) 2 min. after addition of 3-methyl-2-buten-1-ol to (b) ; (d) after 2h of reaction, THA-4 (●, minor), THA-6 (♦, major), and $(THA)_3[SbW_9O_{33}(^tBuSiO)_3Ti(OCH_2CH=C(CH_3)_2)]$ (■, minor). The doublet at 1.11 ppm belongs to free 2-propanol.

UV–Vis Spectroscopy. The UV–Vis spectra of complexes **3** and **4** in acetonitrile are dominated by a strong absorption in the UV domain due to the $W^{6+} \leftarrow O^{2-}$ ligand-to-metal charge transfers. Upon addition of aqueous H_2O_2 (10 eq) the differences are tenuous but proceeding to the subtraction of the spectra before and after the addition shed light to interesting modifications. In both cases, a new absorption band was observed, which was centered at 264 nm for **3** and at 262 nm for **4** (Figure 6 and Figure S6). On the basis of the NMR results discussed above, these bands could tentatively be attributed to the interaction of H_2O_2 with the tetrahedral Ti centers in a η^1 fashion, as proposed by Bonino et al,[63] thus generating the colorless Ti-(η^1-OOH) species. In the case of **3**, the shape of the band suggests the presence of a supplementary absorption around 350 nm. This could reveal the formation of a small amount of Ti-(η^2-O_2) peroxide species as the result of an acid-base equilibrium with Ti-(OOH) species. In order to elucidate the generation of the Ti-(η^2-O_2) species in our systems we proceeded to Raman spectroscopy analysis.

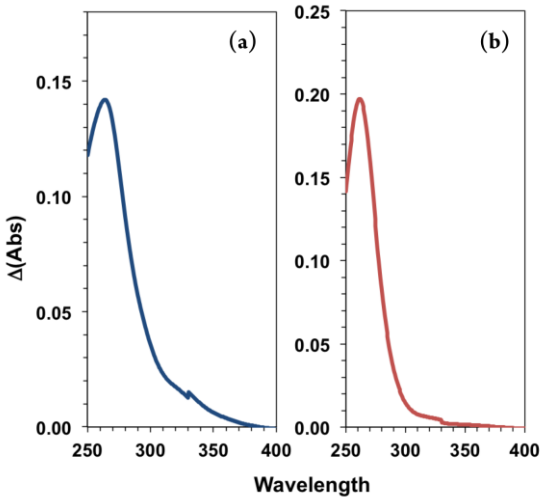

Figure 6. Results of subtraction of UV-Vis spectra after and before addition of 10 eq. of aqueous H_2O_2 (a) to $(THA)_3[PW_9O_{34}(^tBuSiO)_3Ti(O^iPr)]$, THA-3, in acetonitrile, and (b) to $(THA)_3[SbW_9O_{33}(^tBuSiO)_3Ti(O^iPr)]$, THA-4, in acetonitrile.

Raman spectroscopy. To obtain a satisfying signal-to-noise ratio we prepared 60 mM solutions of **3** and **4** in acetonitrile and we used a 458 nm laser source (see the experimental section). The Raman spectra are also dominated by two W-specific modes at 970 cm^{-1} and 991 cm^{-1}. The intrinsically weaker Ti-specific modes are either undetectable or covered by those of the POM framework. Upon addition of H_2O_2 two different behaviors were observed. In the case of **THA-3**, at this higher concentration, the solution turned yellow (due to the LMCT $Ti^{4+} \leftarrow O_2^{2-}$ absorption) and the Raman analysis revealed the appearance of a sharp and intense band at 618 cm^{-1} indicative of the formation of a Ti–peroxide species. Upon subsequent addition of 3-methyl-2-buten-1-ol this band widened while remaining centered at 620 cm^{-1} (Figure 7, left). This slight modification suggests some rearrangement in the coordination sphere, probably due to the presence of the allylic alcohol. When the order of addition of the reagents was reversed the wide peak at 620 cm^{-1} was immediately observed. In both cases, the bands corresponding to the

Ti–peroxide species and 3-methyl-2-buten-1-ol collapsed over time. ^{1}H NMR analysis of the resulting solutions revealed that the oxidation reaction afforded a 1:1 mixture of epoxide and triol (the ratio increased to 2:1 when H_2O_2 was added after the olefin). In addition, ^{31}P NMR analysis revealed that a small amount of the POM framework was degraded. It is worth noting that the intensity of the mode at 618 cm^{-1} cannot be used for quantitative purposes since it is resonance-enhanced. In the case of **THA-4**, *no color change* was observed upon addition of H_2O_2 and no clear formation of a band at 618 cm^{-1} was observed. Only bubbles appeared at the laser beam spot, a sign of hydrogen peroxide disproportionation.[67] Notably, when H_2O_2 was added to a mixture of **THA–4** and 3-methyl-2-buten-1-ol, no bands were detectable around 620 cm^{-1} and only the band assigned to the olefin collapsed over time (Figure 7, right). NMR analysis of this latter solution clearly indicated a higher selectivity for epoxide (ca. 80%) that matched the one obtained when running catalysis (Table 2).

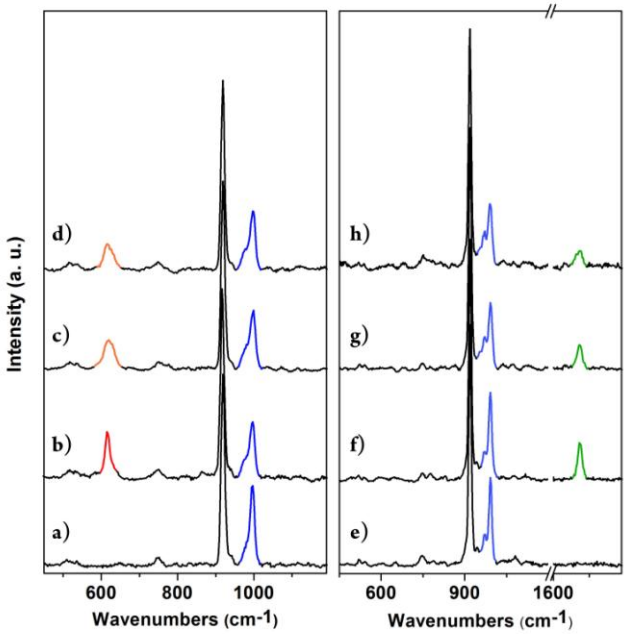

Figure 7. Raman spectra of (a) THA–3 in acetonitrile; (b) after addition of 10 eq. of H_2O_2 to (a); (c) 2 min. after addition of 12 eq. of 3-methyl-2-buten-1-ol to (b); (d) when reagents addition was reversed; (e) THA–4 in acetonitrile, (f) after addition of 12 eq. of 3-methyl-2-buten-1-ol to (e); (g) 2 min. after addition of 10 eq. of H_2O_2 to (f); (h) after 30 min. Colors: blue for the W-specific modes, red and orange for the Ti-peroxide and green for specific mode from 3-methyl-2-buten-1-ol (C=C bond, 1677 cm^{-1}). The spectra have been baseline corrected and normalized to the acetonitrile vibration mode at 910 cm^{-1}.

From these results, it can be assumed that (i) the formation of a Ti(η^2-O_2) peroxide complex is not a prerequisite for epoxidation to occur and either a Ti–(OOH) hydroperoxide intermediate represents the active species, and (ii) in the specific cases of our titanium-polyoxotungstates derivatives **3** and **4,** the equilibrium between Ti–(OOH) and Ti(η^2-O_2) complexes is most probably correlated with the acid–base equilibria that are involved in partial hydrolysis of the siloxy component and/or the polyoxotungstate framework. Whereas the ability of titanium in TS–1 to accommodate coordination numbers higher than four is supported by XANES and EXAFS studies,[68] this is very unlikely (at least energetically unfavorable) in **3** and **4** due to the rigidity imposed by the polyoxotungstate frameworks. Therefore, in the case of the tungstophosphate system (**THA-3**) the formation of Ti(η^2-O_2) peroxide is probably related to the partial hydrolysis of the siloxy part whereby the breaking of a SiO–Ti bond decreases the geometrical constraints around the titanium center. On the contrary, the higher stability of the tungstoantimonate system (**THA-4**) towards hydrolysis of the WO–Si bonds disfavors the formation of titanium peroxide and we can assume that the titanium–hydroperoxide is merely the only active species in the reaction mixture. It should be kept in mind that the absence of a sharp band at 618 cm^{-1} in that case does not exclude the possibility to form *undetectable* amount of

Ti(η^2-O_2) peroxide that could be responsible for the activity. However, the observed production of a much lower amount of triol and the higher catalytic activity observed for **4** compared to **3**, as depicted by initial rate values (r_0= 0.38 mM/min for **3** and r_0= 1.43 mM/min for **4** when applying the catalytic conditions reported in Table 2, entry 3), tend to confirm that Ti–(OOH) is the active species (Scheme 2). In the absence of olefin, the photodissociation of the Ti-OOH moiety, probably enhanced by the laser source, generates a Ti-hydroxyl function and O_2, which escapes as bubbles.[67,69]

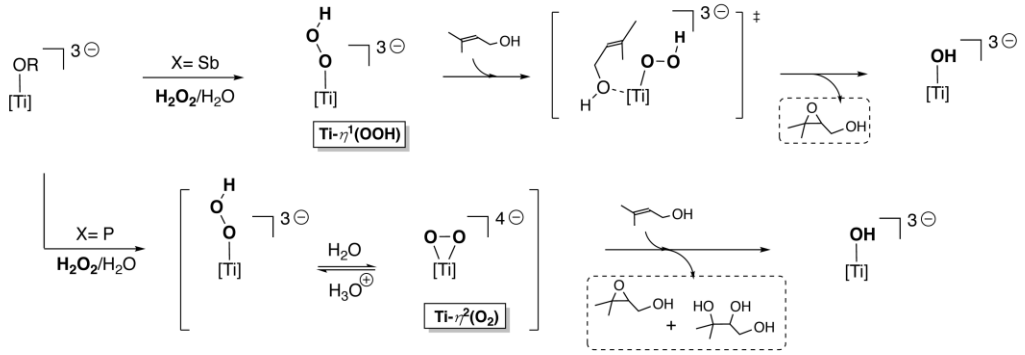

Scheme 2. Proposed reaction schemes for the reactions of 4 (X= Sb, top) and 3 (X= P, bottom) with H_2O_2 and 3-methyl-2-buten-1-ol. Brackets around Ti atom stand for ligand 2 (X= Sb) and for ligand 1 either complete or partially degraded (X= P).

2.4. Kinetic Studies.

We also monitored the catalytic reaction progress by NMR spectroscopy in order (i) to probe the stability of the catalyst, and (ii) to gain understanding on the kinetics. Obviously, a prerequisite for accurate determination of the substrate concentration dependence is that the catalyst maintains a constant activity over time. Hence, to probe the stability of the catalyst system we first performed two runs, with different initial substrate concentrations, but the same

"excess" value. In a reaction exhibiting a 1 to 1 stoichiometry between two reactants, the concentrations are related to each other through this "excess [xs]" value (expressed in M) that remains constant over the course of the reaction. The "same excess" protocol is one of the mechanistic tools from Reaction Progress Kinetic Analysis (RPKA), a methodology which aims at analyzing complex catalytic reactions from a minimal number of experiments.[70,71] The significance of the same excess protocol is that two reactions carried out at different initial concentrations, like entries 2 and 3 in Table 3, represent an identical reaction started from different points. Indeed, when the substrate concentrations for the reaction in entry 2 equal those of the reaction in entry 3, the two kinetic profiles should fall on top of one other providing that *no extra* process other than the intrinsic kinetics influences the reaction rate. Comparison of the kinetic profiles is made possible by shifting the curve for entry 3 (as indicated by the arrows in Figure 8a) in order to intercept the one for entry 2 at the point where concentrations are the same. Figure 8b clearly indicates that from this point onward the two reactions do not exhibit the same temporal substrate concentrations. At this point, three main features distinguish the reaction of entry 2 from that of entry 3: (i) the catalyst has already performed several turnovers, (ii) the products of the reaction, epoxide and water, have accumulated in the reaction medium, and (iii) a larger quantity of water is present from the beginning due to the higher hydrogen peroxide concentration used. Indeed, the higher rate of conversion that is observed for reaction 3 compared to that of reaction 2 at the same substrate concentrations correlates to a catalyst deactivation, which can result either from the formation of an inactive form (or leaching) or from a product inhibition.

Table 3. Catalytic conditions used, with same [xs] values, for the NMR monitoring of the epoxidation of 3-methyl-2-buten-1-ol with H_2O_2 catalyzed by THA-4. [a]

Entry	$[H_2O_2]_0$ (mM)	$[Olefin]_0$ (mM)	[xs] (mM)	%Conv [b]	Selectivity (%) [c]		
					Epox	Triol	Ald
1	260	260	-	57 (21 h)	80	8.2	9.3
2	270	420	150	91 (12 h)	82	10.2	7.7
3	160	310	150	96 (4 h)	87	7.1	2.8
4[d]	160	310	150	92 (5 h)	71.7	9.9	6.1
5[e]	160	310	150	98 (4 h)	84.3	10.4	4.9

[a] All reactions were carried out in acetonitrile–d_3 at 298K with [**THA–4**]$_0$= 2.6 mM. [b] Conversion is observed after the time indicated under brackets, based on the concentration of [olefin]. [c] Undefined side products are not listed. [d] Reaction carried out with addition of water. [e] Reaction carried out with addition of 2,3-epoxy product.

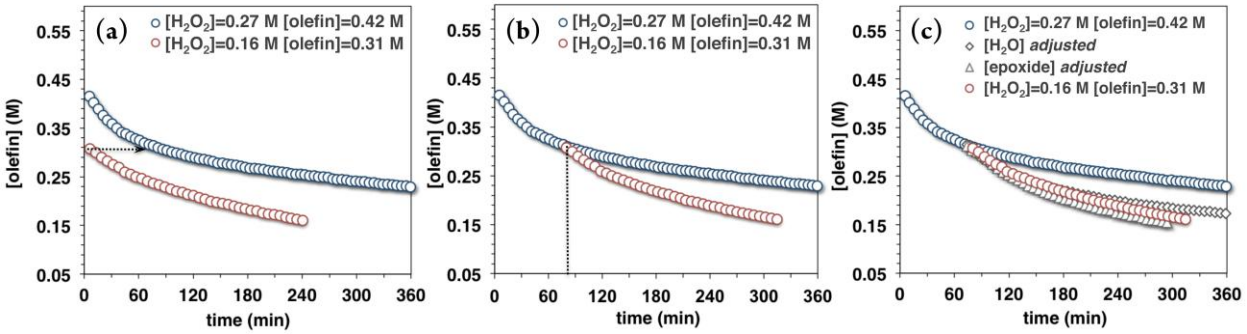

Figure 8. Plots of the concentration of 3–methyl–2–buten–1–ol as a function of the time in the oxidation by H_2O_2 in CD_3CN at room temperature, catalyzed by $(THA)_3[SbW_9O_{33}(^tBuSiO)_3Ti(O^iPr)]$, THA–4 ; (a) reactions of entries 2 and 3 using the « same excess » protocole; (b) the red profile is time–adjusted to the point at which concentrations in $[olefin]_t$ and $[H_2O_2]_t$ are the same in the two experiments; (c) comparison of the kinetic profiles for entry 4 ($[H_2O]$ adjusted, ◇) and for entry 5 ([epoxide] adjusted, △).

Water has been often reported as a main factor of inhibition for titanium-based oxidation catalysis. Thus, we carried out two supplementary experiments for which the initial substrate concentrations and the *water* concentration (entry 4) or the *epoxide* concentration (entry 5) are identical to those of the reaction in entry 2 at the point of intersection. Comparison of the kinetic profiles (i) shows that *accumulated* water does not significantly change the kinetic profile at the beginning of the catalysis, but that a deviation could be observed over time, (ii) indicates that *accumulated* epoxide does not change either the kinetic profile in a significant extent (Figure 8c). Hence, we can conclude that the difference between the reaction profiles of entries 2 and 3 results from a partial catalyst degradation leading to the formation of less or inactive species.

This is consistent with the fact that the polyoxotungstates **1** and **2** undergo partial hydrolysis when the hydrogen peroxide concentration is too high (as shown in Figure S3 and Scheme S2). Using an excess of olefin and decreasing $[H_2O_2]_i$ and $[H_2O]_i$ resulted in almost complete conversion, up to 96% in 4 h when a 1:60:120 catalyst:H_2O_2:olefin mixture was used (entry 3). These conditions also afforded an increased turnover frequency value over the reaction time (mean TOF= 24 h^{-1}). It is also not surprising to observe that the selectivity towards epoxide slightly dropped when a larger amount of water is present (entry 4).

More interestingly, monitoring the reaction progress by ^{1}H NMR also allows to draw a picture of the kinetics along the catalysis, *i.e.* along the *in situ* reagents concentration. To do so, the temporal concentration data have first to be converted mathematically in order to obtain the reaction rate evolution over time (Figure S7). Then, plotting the rate *vs* substrate concentration gives a graphical equation of the reaction. Figure 9 displays a graphical rate equation of the data obtained for entry 3 as rate *vs* [olefin] and reveals a linear behavior, in the range of 0.31 to 0.2M,

with a nonzero intercept (below 0.2M, the observed deviation could be either attributed to a change of the kinetics at lower concentrations or to an increased noise due to the mathematical manipulations). This result can be rationalized by expressing the rate law as $k\cdot[H_2O_2]$. Considering the definition of [*xs*], we can formulate the concentration of H_2O_2 as $[H_2O_2]$= [olefin] – [*xs*], and thereof the rate law as $k\cdot$[olefin] – $k\cdot$[*xs*]. This defines the equation of the straight line depicted in Figure 9. The slope of the linear portion gives $k = 8.79\ 10^{-3}$ min^{-1} and the y-intercept gives –1.45 mM/min, which is in good agreement with calculated – $k\cdot$[*xs*]= –1.32 mM/min (see also Figure S7). This indicates that (i) the reaction is first-order in $[H_2O_2]$ and (ii) the reaction is pseudo zero-order in [olefin] (saturation kinetics in [olefin]). The rate law is consistent with addition of H_2O_2 being the turnover-limiting step and $[SbW_9O_{33}(^tBuSiO)_3Ti(OCH_2CH{=}C(CH_3)_2)]^{3-}$ being the catalyst resting state, which has been clearly demonstrated by NMR monitoring. We can also underline that the constancy of the kinetic regime tends to indicate that the catalyst does not undergo significant degradation under the catalytic conditions used for entry 3. In this study, the possibility to monitor the reaction progress by NMR and the rather high selectivity of the reaction were the prerequisites to make use of the RPKA methodologies in order to look inside the reaction to get a full picture of the catalytic mechanism instead of the snapshots provided by conventional kinetic methods such as measurements of the initial rate.

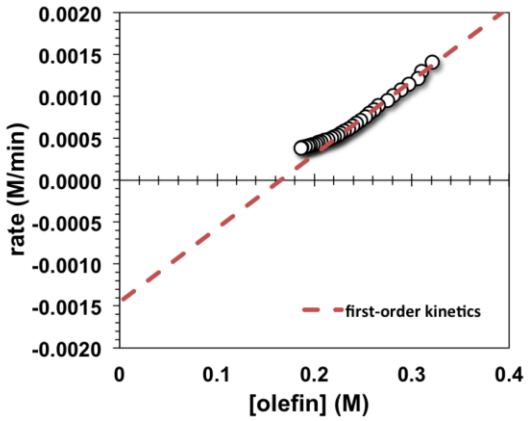

Figure 9. Graphical rate equation (Table 3, entry 3): rate vs 3-methyl-2-buten-1-ol concentration, [olefin]. The linear behavior with non-zero intercept related to value of [xs] indicates a first-order in [H_2O_2] and a zero-order in [3-Me-2-buten-1-ol].

These preliminary kinetic studies proved the ability of the titanium–based polyoxotungstate **4** to catalyze the epoxidation of nucleophilic allylic alcohols with aqueous solution of hydrogen peroxide at room temperature. One requirement lies in the fact that concentration in hydrogen peroxide should remain low enough to avoid partial hydrolysis and maintain the integrity of the catalyst over the reaction. We should remind at this stage that one of the factors governing the catalytic performances of TS-1 lies in the size and hydrophobic nature of the pores of its crystalline framework, which promote the physisorption of apolar substrates and ensure slow diffusion of hydrogen peroxide and a limited amount of water inside the pore volume.[72,73] No homogeneous system can compare to that. However, **THA-4** is particularly interesting because the fact that Ti(IV) site is not prone to expand its coordination sphere is probably the reason why inhibition of the active site by water molecules is minimized. Above all, our studies reveal that the Ti-hydroperoxide species formed is not very reactive for the conversion of non-functionalized alkenes under our catalysis conditions. Therefore, efforts must be made to

increase the concentration of olefin at the active center and if possible to increase its electrophilic character. Further catalytic tests, recycling studies, as well as kinetic studies will be undertaken in order to improve the catalytic performance and the scope of applications of our systems.

3. CONCLUSIONS

The silanol–decorated polyoxotungstates $[XW_9O_{34-x}(^t\text{BuSiOH})_3]^{3-}$ (X= P, x=0, **1**; X= Sb, x=1, **2**) have been used as original ligands in an approach to modeling active sites of titanium-containing heterogeneous epoxidation catalysts. The most notable feature of these ligands lies in the pre-organization of the silanol functionalities, which leads to complexes with constrained geometry. The titanium-isopropoxide complexes $(n\text{-Hex}_4\text{N})_3[\alpha\text{-A-PW}_9\text{O}_{34}(^t\text{BuSiO})_3\text{Ti}(O^i\text{Pr})]$ (**THA-3**) and $(n\text{-Hex}_4\text{N})_3[\alpha\text{-B-SbW}_9\text{O}_{33}(^t\text{BuSiO})_3\text{Ti}(O^i\text{Pr})]$ (**THA-4**) have been synthesized and characterized using NMR spectroscopy and single-crystal X-ray diffraction. The complexes proved relevant models for single-site silica-supported titanium catalysts, especially the defective open-lattice sites that are present in the MFI framework of the titanium-silicalite TS-1. Monitoring by NMR and Raman spectroscopies the reaction between **THA-3** / **THA-4** and aqueous solutions of hydrogen peroxide showed that a titanium metal atom in such constrained and confined environments activates H_2O_2 to form a Ti-hydroperoxide Ti-(OOH) intermediate. Importantly, this work shed light to the fact that this latter proved to be the active species responsible for high epoxide selectivity in allylic alcohols oxidation with H_2O_2. In our systems, the evolution to Ti(η^2-O_2) peroxide species is only made possible by the limited solution stability of **3** which undergoes partial hydrolysis of the siloxy functionalities and thus releases the geometric stress around the titanium centre. In that case, formation of Ti(η^2-O_2) peroxide correlates to the increase for 1,2,3-butane-triol selectivity as a consequence of the concomitant

release of protons that catalyze the oxirane opening of the *in situ* formed epoxide. In the case of the more stable **THA-4**, the evolution to Ti(η^2-O_2) peroxide was not detected by Raman spectroscopy and Ti–(OOH) species reacted with allylic alcohol to selectively produce epoxide whereas H_2O_2 decomposition may occur in the absence of olefin. Reaction progress kinetic analysis methodology was also meaningful to map the catalytic mechanism over the course of the reaction and to provide evidence for catalyst integrity at low concentration of H_2O_2. To the best of our knowledge, **THA–4** represents the first example of a soluble titanium complex structurally modeling the open sites of TS-1 and able to carry out the epoxidation of olefin with aqueous solutions of H_2O_2 without the need of embedment into a hydrophobic environment such as polymers. Whereas classical models of heterogeneous titanium catalysts are reported to deactivate in contact with water, **THA-4** shows a higher stability, most probably due to the hydrophobicity provided by the surrounding tetrahexylammonium cations and t-butyl groups, but also to the rigidity of the POM framework, which disfavors the increase of the titanium coordination number.

4. EXPERIMENTAL SECTION

General Procedures. The lacunary polyoxotungstates $K_9[\alpha\text{-A-}PW_9O_{34}]$ and $Na_9[\alpha\text{-B-}SbW_9O_{33}]$ were prepared as reported in the literature.[74] Their silanol derivatives $(n\text{-}Hex_4N)_3[(\alpha\text{-A-}PW_9O_{34})(tBuSiOH)_3]$ **(THA–1)** and $(n\text{-}Hex_4N)_3[(\alpha\text{-B-}SbW_9O_{33})(^tBuSiOH)_3]$ **(THA–2)** were prepared according to modified procedures (*vide infra*).[75,76] All manipulations were conducted under a nitrogen atmosphere using standard Schlenk techniques. Tetrahydrofuran and acetonitrile were dried using solvent purification systems or by distillation under argon from appropriate drying agents. All solvents, including deuterated acetonitrile, were then degassed by several

freeze-pump-thaw cycles and stored over activated molecular sieves. Titanium tetra-isopropoxide, $Ti(O^iPr)_4$, hydrogen peroxide (30 wt.% in H_2O), *m*-chloroperoxybenzoic acid (*m*-CPBA) and olefins were purchased from Sigma, Alfa or Acros and used as received. (3,3-Dimethyloxiran-2-yl)methanol was synthesized from 3-methyl-2-buten-1-ol and *m*-CPBA according to a reported procedure.[77] ^1H NMR and $^{31}P\{^1H\}$ NMR spectra were obtained at room temperature in 5 mm o.d. tubes on a Bruker AvanceII 300 spectrometer equipped with a QNP probehead or on a Bruker AvanceIII 600 spectrometer equipped with a BBFO probehead. For ^1H, chemical shifts are referenced with respect to tetramethylsilane by using the solvent signals as secondary standard. For $^{31}P\ \{^1H\}$, chemical shifts were measured by the substitution method and are given with respect to 85% H_3PO_4. The Raman spectra were recorded using a Horiba Jobin Yvon LabRam HR 800 spectrometer equipped with edge filters, a 600 lines/mm grating and a Peltier cooled CCD detector. The excitation wavelength was the 458 nm line of an Ar^+ Laser (Innova 90C, Coherent Inc.). The laser power at the sample was around 400μW. Raman scattering was collected via an Olympus microscope equipped with a long working distance 50× objective, allowing a laser spot size of about 5 μm. The time of exposition was about 240s. All the spectra have been baseline subtracted and normalized to the acetonitrile band at 920 cm^{-1}. Elemental analyses were performed by the « Service de microanalyses » from the ICSN–CNRS, Gif-sur-Yvette, France.

Synthesis of $THA_3[PW_9O_{34}(^tBuSiOH)_3]$ (THA–1). $K_9[\alpha\text{-A-}PW_9O_{34}]$ (1.283 g, 0.447 mmol) and $[(C_6H_{13})_4N]Br$ (0.777 g, 1.788 mmol) were placed in a Schlenk tube and, under argon atmosphere, freshly distilled acetonitrile (20 mL) was added. The suspension was first cooled to 0°C for half an hour, then *t*-$BuSiCl_3$ (0.257 g, 1.341 mmol) was added and vigorous stirring was maintained overnight at 0°C. The suspension was allowed to warm to room temperature and then

the solid was filtered off (mixture of KCl, KBr and unreacted reactants). The solution was evaporated to dryness to give a white solid that was washed with ethanol and diethyl ether and finally dried under vacuum. Yield: 1.11 g (69 %). Elemental analysis calcd (%) for $C_{84}H_{186}N_3O_{37}PSi_3W_9$ (3600.18): C 28.02, H 5.21, N 1.17; found: C 27.66, H 5.21, N 1.14. ^{1}H NMR (CD_3CN, 400 MHz, 300 K) δ, ppm: 3.11 (m, 24 H, NC*H*$_2$ THA), 1.63 (m, 24 H, NCH_2CH_2 THA), 1.35 (m, 72 H, $(CH_2)_3CH_3$ THA), 1.00 (s, 27 H, C*H*$_3$ *t*-BuSi), 0.91 (t, $^2J_{H,H}$ = 6.9 Hz; 36 H, CH_2CH_3 THA). $\{^1H\}^{31}$P NMR (CD_3CN, 162 MHz, 300K) δ, ppm: -16.9 (s).

Synthesis of $THA_3[SbW_9O_{33}(^tBuSiOH)_3]$ (THA–2). $Na_9[\alpha\text{-B-}SbW_9O_{33}]$ (2.0 g, 0.699 mmol) and $[(C_6H_{13})_4N]Br$ (0.777 g, 1.788 mmol) were placed in a Schlenk tube and, under argon atmosphere, freshly distilled acetonitrile (25 mL) was added. The suspension was first cooled to 0°C for half an hour, then *t*-$BuSiCl_3$ (0.402 g, 2.096 mmol) was added and vigorous stirring was maintained overnight at 0°C. The suspension was allowed to warm to room temperature and then the solid was filtered off (mixture of NaCl, NaBr and unreacted reactants). The solution was then concentrated to *ca*. 12 mL and layered by diethyl ether to afford crystals which were filtered off, washed with diethyl ether and dried under vacuum. Yield: 1.30 g (51 %). Elemental analysis calcd (%) for $C_{84}H_{186}N_3O_{36}SbSi_3W_9$ (3674.97): C 27.45, H 5.10, N 1.14; found: C 27.29, H 5.13, N 1.03. ^{1}H NMR (CD_3CN, 400 MHz, 300 K) δ, ppm: 3.11 (m, 24 H, NC*H*$_2$ THA), 1.63 (m, 24 H, NCH_2CH_2 THA), 1.35 (m, 72 H, $(CH_2)_3CH_3$ THA), 1.18 (s, 27 H, C*H*$_3$ *t*-BuSi), 0.91 (t, $^2J_{H,H}$ = 6.9 Hz; 36 H, CH_2CH_3 THA).

Dehydration of THA–1 and THA–2. Samples of $THA_3[PW_9O_{34}(^tBuSiOH)_3]$ and $THA_3[SbW_9O_{33}(^tBuSiOH)_3]$ were dehydrated by heating at 210°C for 3 h under dynamic vacuum (10^{-3} mbar) and stored under inert atmosphere before use. Complete dehydration may be

controlled by thermo gravimetric profiles that show no mass loss below 270°C. NMR analyses after heating treatment indicated that the structures were not modified.

Synthesis of $THA_3[PW_9O_{34}(^tBuSiO)_3Ti(O^iPr)]$ (THA–3). Dehydrated $THA_3[PW_9O_{34}(^tBuSiOH)_3]$ (0.581 g, 0.161 mmol) was placed in a Schlenk tube and, under argon atmosphere, dried THF (10 mL) was added. At room temperature $Ti(O^iPr)_4$ (48 μL, 0.161 mmol) was then added and the resulting solution was stirred overnight. The solution was then concentrated to half of its volume and layered by diethyl ether to induce crystallization of the compound. The deposited crystals were collected, washed with diethyl ether and dried under vacuum to yield 0.34 g (57 %) of $THA_3[PW_9O_{34}(^tBuSiO)_3Ti(O^iPr)]$. Elemental analysis calcd (%) for $C_{87}H_{190}N_3O_{38}PSi_3TiW_9$ (3704.12): C 28.21, H 5.17, N 1.13; found: C 28.02, H 5.28, N 1.01. ^{1}H NMR (CD_3CN, 400 MHz, 300 K) δ, ppm: 4.70 (sept, $^3J_{H,H}$= 6.1 Hz ; 1H, Ti(OC*H*$(CH_3)_2$), 3.11 (m, 24 H, NC*H*$_2$ THA), 1.63 (m, 24 H, NCH_2CH_2 THA), 1.35 (m, 72 H, $(CH_2)_3CH_3$ THA), 1.26 (d, $^3J_{H,H}$= 6.1 Hz ; 6H, Ti(OCH(C*H*$_3)_2$), 1.04 (s, 27 H, C*H*$_3$ *t*-BuSi), 0.91 (t, $^2J_{H,H}$ = 6.9 Hz; 36 H, CH_2CH_3 THA). $\{^1H\}^{31}$P NMR (CD_3CN, 162 MHz, 300K) δ, ppm: -16.93 (s). Crystals suitable for X-ray analysis were grown by slowly diffusing diethylether in a tetrahydrofuran solution at room temperature.

$THA_3[SbW_9O_{33}(^tBuSiO)_3Ti(O^iPr)]$ (THA–4) was prepared following the same procedure as for the synthesis of **THA–3**. This compound was always isolated with *ca*. 5% of the dimeric form **THA-6**. ^{1}H NMR (CD_3CN, 400 MHz, 300 K) δ, ppm: 4.55 (sept, $^3J_{H,H}$= 6.1 Hz; 1H, Ti(OC*H*$(CH_3)_2$), 3.11 (m, 24 H, NC*H*$_2$ THA), 1.63 (m, 24 H, NCH_2CH_2 THA), 1.35 (m, 72 H, $(CH_2)_3CH_3$ THA) overlapping with 1.32 (d, $^3J_{H,H}$= 6.1 Hz; 6H, Ti(OCH(C*H*$_3)_2$), 1.18 (s, 27 H, C*H*$_3$ *t*-BuSi), 0.91 (t, $^2J_{H,H}$ = 6.9 Hz; 36 H, CH_2CH_3 THA). Crystals suitable for X-ray analysis were grown by slowly diffusing diethylether in a tetrahydrofuran solution at room temperature.

Synthesis of $THA_6[SbW_9O_{33}(^tBuSiO)_3Ti]_2O$ (THA–6). The same procedure was followed: dehydrated $THA_3[SbW_9O_{33}(^tBuSiOH)_3]$ (0.500 g, 0.136 mmol) was placed in a Schlenk tube and, under argon atmosphere, dried THF (10 mL) was added. At room temperature $Ti(O^iPr)_4$ (41 μL, 0.136 mmol) was then added and the resulting solution was stirred overnight. The volatiles were removed under vacuum and the solid was recrystallized from a solution in *wet* THF layered with *wet* diethyl ether (*wet* meaning not dried). Crystals (suitable for X-ray diffraction) grew after two days standing at room temperature. The crystals were collected, washed with diethyl ether and dried under vacuum (283 mg, 56 %). Elemental analysis calcd (%) for $C_{168}H_{366}N_6O_{73}Sb_2Si_6Ti_2W_{18}$ (7455.63): C 27.06, H 4.95, N 1.13; found: C 27.06, H 4.98, N 0.95. ^{1}H NMR (CD_3CN, 400 MHz, 300 K) δ, ppm: 3.11 (m, 24 H, NC*H*$_2$ THA), 1.63 (m, 24 H, NCH_2CH_2 THA), 1.35 (m, 72 H, $(CH_2)_3CH_3$ THA), 1.15 (s, 27 H, C*H*$_3$ *t*-BuSi), 0.91 (t, $^2J_{H,H}$ = 6.9 Hz; 36 H, CH_2CH_3 THA).

X-ray Crystallography. A single crystal of each compound was selected, mounted onto a cryoloop, and transferred in a cold nitrogen gas stream. Intensity data were collected with a Bruker Kappa-APEXII diffractometer with graphite-monochromated Mo-Kα radiation (λ = 0.71073 Å). Data collections were performed with APEX2 suite (BRUKER). Unit-cell parameters refinement, integration and data reduction were carried out with SAINT program (BRUKER). SADABS (BRUKER) was used for scaling and multi-scan absorption corrections. In the WinGX suite of programs,[78] the structures were solved with SHELXT–14 program[79] and refined by full–matrix least-squares methods using SHELXL–14.[80]

CCDC–1581183 contains the supplementary crystallographic data of compound THA-3 for this paper. These data can be obtained free of charge from The Cambridge Crystallographic Data Centre via www.ccdc.cam.ac.uk/data–request/cif.

NMR Monitoring of the Catalytic Olefin Epoxidation. In a typical procedure, a screw capped 5 mm o.d. NMR tube under argon was charged with 6.85 mg of THA-4 (to get a 2.6 mM solution) and 665 μL of dry acetonitrile–d_3 (for each catalytic experiment, the volume of acetonitrile was adjusted to obtain the desired reactant concentrations). Then, 21 μL of 3-methyl-2-buten-1-ol (affording a 0.31 M solution) and 11 μL of a 30 wt.% aqueous solution of H_2O_2 (leading to a 0.16 M solution) were successively added to the mixture. Each step was monitored at 300 K by ^{1}H NMR on a Bruker AvanceIII 600 spectrometer equipped with a BBFO probehead. The acquisition parameters (relaxation delays) have been optimized to ensure accurate integration. The NMR data set (integral measurements) was fitted to a polynomial function to generate a full profile, when possible. The functions were then differentiated to obtain rate versus time data (see Figure S7).

ASSOCIATED CONTENT

ORCID

Lise-Marie Chamoreau: 0000-0002-9755-7459

Geoffroy Guillemot: 0000-0002-2711-8514

Author Contributions

The manuscript was written through contributions of all authors. All authors have given approval to the final version of the manuscript.

Notes

The authors declare no competing financial interest

ACKNOWLEDGMENT

The authors want to acknowledge and to dedicate this work to Professor Pierre Gouzerh for helpful discussions. T. Zhang wants to acknowledge the Sorbonne Universités – China Scholarship Council program for a PhD grant.

REFERENCES

(1) Perego, G.; Bellussi, G.; Corno, C.; Taramasso, M.; Buonomo, F.; Esposito, A. Titanium-Silicalite: A Novel Derivative in the Pentasil Family. In *Studies in Surface Science and Catalysis* **1986**, *28*, 129–136.

(2) *Liquid Phase Oxidation via Heterogeneous Catalysis: Organic Synthesis and Industrial Applications*; Clerici, M. G.; Kholdeeva, O. A., Ed.; Wiley, New Jersey, 2013.

(3) Arends, I. W. C. E.; Sheldon, R. A.; Wallau, M.; Schuchardt, U. Oxidative Transformations of Organic Compounds Mediated by Redox Molecular Sieves. *Angew. Chem. Int. Ed. Engl.* **1997**, *36*, 1144–1163.

(4) Kholdeeva, O. A. Recent Developments in Liquid-Phase Selective Oxidation Using Environmentally Benign Oxidants and Mesoporous Metal Silicates. *Catal. Sci. Technol.* **2014**, *4*, 1869–1889.

(5) *Catalytic Oxidations with Hydrogen Peroxide as Oxidant*; Strukul, G., Ed.; Kluwer Academic: Dordrecht, The Netherlands, 1992.

(6) Lane, B. S.; Burgess, K. Metal-Catalyzed Epoxidations of Alkenes with Hydrogen Peroxide. *Chem. Rev.* **2003**, *103*, 2457–2474.

(7) Clerici, M. G. The Activity of Titanium Silicalite-1 (TS-1): Some Considerations on Its Origin. *Kinet. Catal.* **2015**, *56*, 450–455.

(8) Bregeault, J.-M. Transition-Metal Complexes for Liquid-Phase Catalytic Oxidation: Some Aspects of Industrial Reactions and of Emerging Technologies. *Dalton Trans.* **2003**, 3289–3302.

(9) To, J.; Sokol, A. A.; French, S. A.; Catlow, C. R. A. Hybrid QM/MM Investigations into the Structure and Properties of Oxygen-Donating Species in TS-1. *J. Phys. Chem. C* **2008**, *112*, 7173–7185.

(10) Quadrelli, E. A.; Basset, J. M. On Silsesquioxanes' Accuracy as Molecular Models for Silica-Grafted Complexes in Heterogeneous Catalysis. *Coord. Chem. Rev.* **2010**, *254*, 707–728.

(11) Abbenhuis, H. C. L. Advances in Homogeneous and Heterogeneous Catalysis with Metal-Containing Silsesquioxanes. *Chem. – Eur. J.* **2000**, *6*, 25–32.

(12) Ward, A. J.; Lesic, R.; Masters, A. F.; Maschmeyer, T. Silsesquioxanes as Molecular Analogues of Single-Site Heterogeneous Catalysts. *Proc R Soc A* **2012**, *468*, 1968–1984.

(13) Guillemot, G.; Matricardi, E.; Chamoreau, L.-M.; Thouvenot, R.; Proust, A. Oxidovanadium(V) Anchored to Silanol-Functionalized Polyoxotungstates: Molecular Models for Single-Site Silica-Supported Vanadium Catalysts. *ACS Catal.* **2015**, *5*, 7415–7423.

(14) Lamberti, C.; Bordiga, S.; Arduino, D.; Zecchina, A.; Geobaldo, F.; Spanó, G.; Genoni, F.; Petrini, G.; Carati, A.; Villain, F.; Vlaic, G. Evidence of the Presence of Two Different Framework Ti(IV) Species in Ti−Silicalite-1 in Vacuo Conditions: An EXAFS and a Photoluminescence Study. *J. Phys. Chem. B* **1998**, *102*, 6382–6390.

(15) Le Noc, L.; Trong On, D.; Solomykina, S.; Echchahed, B.; Béland, F.; Cartier dit Moulin, C.; Bonneviot, L. Characterization of Two Different Framework Titanium Sites and Quantification of Extra-Framework Species in TS-1 Silicalites. *Stud. Surf. Sci. Catal.* **1996**, *101*, 611–620.

(16) Skowronska-Ptasinska, M. D.; Vorstenbosch, M. L. W.; van Santen, R. A.; Abbenhuis, H. C. L. Titanium Silsesquioxanes Grafted on Three-Dimensionally Netted Polysiloxanes: Catalytic Ensembles for Epoxidation of Alkenes with Aqueous Hydrogen Peroxide. *Angew. Chem. Int. Ed.* **2002**, *41*, 637–639.

(17) Zhang, L.; Abbenhuis, H. C. L.; Gerritsen, G.; Bhriain, N. N.; Magusin, P. C. M. M.; Mezari, B.; Han, W.; van Santen, R. A.; Yang, Q.; Li, C. An Efficient Hybrid, Nanostructured, Epoxidation Catalyst: Titanium Silsesquioxane–Polystyrene Copolymer Supported on SBA-15. *Chem. – Eur. J.* **2007**, *13*, 1210–1221.

(18) Aish, E. H.; Crocker, M.; Ladipo, F. T. Tripodal Titanium Silsesquioxane Complexes Immobilized in Polydimethylsiloxane (PDMS) Membrane: Selective Catalysts for Epoxidation of Cyclohexene and 1-Octene with Aqueous Hydrogen Peroxide. *J. Catal.* **2010**, *273*, 66–72.

(19) Kozhevnikov, I. V. Catalysis by Polyoxometalates; Wiley, Chichester, England, 2002.

(20) Mizuno, N.; Yamaguchi, K.; Kamata, K. Epoxidation of Olefins with Hydrogen Peroxide Catalyzed by Polyoxometalates. *Coord. Chem. Rev.* **2005**, *249*, 1944–1956.

(21) Sarma, B. B.; Efremenko, I.; Neumann, R. Oxygenation of Methylarenes to Benzaldehyde Derivatives by a Polyoxometalate Mediated Electron Transfer–Oxygen Transfer Reaction in Aqueous Sulfuric Acid. *J. Am. Chem. Soc.* **2015**, *137*, 5916–5922.

(22) Wang, S.-S.; Yang, G.-Y. Recent Advances in Polyoxometalate-Catalyzed Reactions. *Chem. Rev.* **2015**, *115*, 4893–4962.

(23) Contant, R.; Herve, G. The Heteropolyoxotungstates: Relationships Between Routes of Formation and Structures. *Rev. Inorg. Chem.* **2011**, *22*, 63–112.

(24) Proust, A.; Thouvenot, R.; Gouzerh, P. Functionalization of Polyoxometalates: Towards Advanced Applications in Catalysis and Materials Science. *Chem. Commun.* **2008**, 1837–1852.

(25) Mazeaud, A.; Ammari, N.; Robert, F.; Thouvenot, R. Coordination Chemistry of Polyoxometalates: Rational Synthesis of the Mixed Organosilyl Derivatives of Trivacant Polyoxotungstates α-A-$[PW_9O_{34}(t\text{BuSiO})_3(\text{RSi})]^{3-}$ and α-B-$[AsW_9O_{33}(t\text{BuSiO})_3(\text{HSi})]^{3-}$. *Angew. Chem.-Int. Ed. Engl.* **1996**, *35*, 1961–1964.

(26) Dong, J.; Zhu, H.; Xiang, Y.; Wang, Y.; An, P.; Gong, Y.; Liang, Y.; Qiu, L.; Zheng, A.; Peng, X.; Lin, M.; Xu, G.; Guo, Z.; Chen, D. Toward a Unified Identification of Ti Location in the MFI Framework of High-Ti-Loaded TS-1: Combined EXAFS, XANES, and DFT Study. *J. Phys. Chem. C* **2016**, *120*, 20114–20124.

(27) Crocker, M.; Herold, R. H. M.; Crocker, M.; Orpen, A. G. Synthesis and Structural Characterisation of Tripodal Titanium Silsesquioxane Complexes: A New Class of Highly Active Catalysts for Liquid Phase Alkene Epoxidation. *Chem. Commun.* **1997**, *24*, 2411–2412.

(28) Maschmeyer, T.; Klunduk, M. C.; Martin, C. M.; Shephard, D. S.; Thomas, J. M.; Johnson, B. F. G. Modelling the Active Sites of Heterogeneous Titanium-Centred Epoxidation Catalysts with Soluble Silsesquioxane Analogues. *Chem. Commun.* **1997**, *19*, 1847–1848.

(29) Steffey, B. D.; Fanwick, P. E.; Rothwell, I. P. Solid State Structure of the Tantalum Bis-Aryl Compounds $Ta(OAr\text{-}2,6R_2)_3(C_6H_5)_2$ (R = CH_3, Pr^i; OAr-2,6R_2 = 2,6-Dialkylphenoxide): Observation of a Lack of Correlation of M-OAr Distances and M-O-Ar Angles for Aryloxide Derivatives of Niobium(V) and Tantalum(V). *Polyhedron* **1990**, *9*, 963–968.

(30) Bouh, A. O.; Rice, G. L.; Scott, S. L. Mono- and Dinuclear Silica-Supported Titanium(IV) Complexes and the Effect of TiOTi Connectivity on Reactivity. *J. Am. Chem. Soc.* **1999**, *121*, 7201–7210.

(31) Kholdeeva, O. A.; Maksimov, G. M.; Maksimovskaya, R. I.; Kovaleva, L. A.; Fedotov, M. A.; Grigoriev, V. A.; Hill, C. L. A Dimeric Titanium-Containing Polyoxometalate. Synthesis, Characterization, and Catalysis of H_2O_2-Based Thioether Oxidation. *Inorg. Chem.* **2000**, *39*, 3828–3837.

(32) Kholdeeva, O. A.; Trubitsina, T. A.; Maksimov, G. M.; Golovin, A. V.; Maksimovskaya, R. I. Synthesis, Characterization, and Reactivity of Ti(IV)-Monosubstituted Keggin Polyoxometalates. *Inorg. Chem.* **2005**, *44*, 1635–1642.

(33) Kato, C. N.; Hayashi, K.; Negishi, S.; Nomiya, K. A Novel Ti–O–Ti Bonding Species Constructed in a Metal-Oxide Cluster $[\{Ti(OH_2)(Ox)\}_2(\mu\text{-}O)(\alpha\text{-}PW_{11}O_{39})]^{5-}$ as a Precatalyst: Epoxidation of Alkenes with Hydrogen Peroxide. *J. Mol. Catal. Chem.* **2007**, *262*, 25–29.

(34) Andrianainarivelo, M.; Corriu, R. J. P.; Leclercq, D.; Mutin, P. H.; Vioux, A. Nonhydrolytic Sol−Gel Process: Aluminum Titanate Gels. *Chem. Mater.* **1997**, *9*, 1098–1102.

(35) Sensarma, S.; Bouh, A. O.; Scott, S. L.; Alper, H. Olefin Epoxidation Catalyzed by an Air Stable-Supported Titanium Catalyst. *J. Mol. Catal. Chem.* **2003**, *203*, 145–152.

(36) Edelmann, F. T.; Gießmann, S.; Fischer, A. Silsesquioxane Chemistry, 4.: Silsesquioxane Complexes of Titanium(III) and Titanium(IV). *J. Organomet. Chem.* **2001**, *620*, 80–89.

(37) Domaille, P. J.; Herva, G.; Taza, A. *Inorg. Synth*. **1990**, *27*, 96.

(38) Aubry, C.; Chottard, G.; Platzer, N.; Bregeault, J. M.; Thouvenot, R.; Chauveau, F.; Huet, C.; Ledon, H. Reinvestigation of Epoxidation Using Tungsten-Based Precursors and Hydrogen Peroxide in a Biphase Medium. *Inorg. Chem.* **1991**, *30*, 4409–4415.

(39) Mimoun, H. Oxygen-Transfer from Inorganic and Organic Peroxides to Organic Substrates – A Common Mechanism. *Angew. Chem.-Int. Ed.* **1982**, *21*, 734–750.

(40) Venturello, C.; D'Aloisio, R.; Bart, J. C. J.; Ricci, M. A New Peroxotungsten Heteropoly Anion with Special Oxidizing Properties: Synthesis and Structure of Tetrahexylammonium Tetra(Diperoxotungsto)Phosphate(3-). *J. Mol. Catal.* **1985**, *32*, 107–110.

(41) Brégeault, J.-M.; Vennat, M.; Laurent, S.; Piquemal, J.-Y.; Mahha, Y.; Briot, E.; Bakala, P. C.; Atlamsani, A.; Thouvenot, R. From Polyoxometalates to Polyoxoperoxometalates and Back Again; Potential Applications. *J. Mol. Catal. Chem.* **2006**, *250*, 177–189.

(42) Salles, L.; Thouvenot, R.; Brégeault, J.-M. Redistribution and Fluxionality in Heteropolyoxoperoxo Complexes: $[PO_4\{M_2O_2(\mu\text{-}O_2)_2(O_2)_2\}_2]^{3-}$ with M = Mo and/or W. *Dalton Trans.* **2004**, *33*, 904–907.

(43) Salles, L.; Aubry, C.; Thouvenot, R.; Robert, F.; Doremieux-Morin, C.; Chottard, G.; Ledon, H.; Jeannin, Y.; Bregeault, J. M. ^{31}P and ^{183}W NMR Spectroscopic Evidence for Novel Peroxo Species in the "$H_3[PW_{12}O_{40}]\cdot yH_2O/H_2O_2$" System. Synthesis and X-Ray Structure of

Tetrabutylammonium (μ-Hydrogen phosphato)bis(μ-peroxo)bis(oxoperoxotungstate)(2-): A Catalyst of Olefin Epoxidation in a Biphase Medium. *Inorg. Chem.* **1994**, *33*, 871–878.

(44) Jallet, V. *Conception de polyoxométallates amphiphiles pour la catalyse d'oxydation en microémulsion*; PhD Thesis, Université Pierre et Marie Curie, 2014.

(45) Kamata, K.; Kotani, M.; Yamaguchi, K.; Hikichi, S.; Mizuno, N. Olefin Epoxidation with Hydrogen Peroxide Catalyzed by Lacunary Polyoxometalate $[\gamma\text{-}SiW_{10}O_{34}(H_2O)_2]^{4-}$. *Chem.- Eur. J.* **2007**, *13*, 639–648.

(46) Server-Carrió, J.; Bas-Serra, J.; González-Núñez, M. E.; García-Gastaldi, A.; Jameson, G. B.; Baker, L. C. W.; Acerete, R. Synthesis, Characterization, and Catalysis of β_3-$[(Co^{II}O_4)W_{11}O_{31}(O_2)_4]$,$^{10-}$ the First Keggin-Based True Heteropoly Dioxygen (Peroxo) Anion. Spectroscopic (ESR, IR) Evidence for the Formation of Superoxo Polytungstates. *J. Am. Chem. Soc.* **1999**, *121*, 977–984.

(47) Antonova, N. S.; Carbó, J. J.; Kortz, U.; Kholdeeva, O. A.; Poblet, J. M. Mechanistic Insights into Alkene Epoxidation with H_2O_2 by Ti- and Other TM-Containing Polyoxometalates: Role of the Metal Nature and Coordination Environment. *J. Am. Chem. Soc.* **2010**, *132*, 7488–7497.

(48) Kholdeeva, O. A. Hydrogen Peroxide Activation over Ti^{IV}: What Have We Learned from Studies on Ti-Containing Polyoxometalates? *Eur. J. Inorg. Chem.* **2013**, *2013*, 1595–1605.

(49) Goto, Y.; Kamata, K.; Yamaguchi, K.; Uehara, K.; Hikichi, S.; Mizuno, N. Synthesis, Structural Characterization, and Catalytic Performance of Dititanium-Substituted γ-Keggin Silicotungstate. *Inorg. Chem.* **2006**, *45*, 2347–2356.

(50) Takahashi, E.; Kamata, K.; Kikukawa, Y.; Sato, S.; Suzuki, K.; Yamaguchi, K.; Mizuno, N. Synthesis and Oxidation Catalysis of a Ti-Substituted Phosphotungstate, and Identification of the Active Oxygen Species. *Catal. Sci. Technol.* **2015**, *5*, 4778–4789.

(51) Nomiya, K.; Sakai, Y.; Matsunaga, S. Chemistry of Group IV Metal Ion-Containing Polyoxometalates. *Eur. J. Inorg. Chem.* **2011**, *2011*, 179–196.

(52) Alloul, L.; Ammari, N.; Mayer, C. R.; Mazeaud, A.; Thouvenot, R. Organic-inorganic hybrids based on polyoxometalates. Part IV: A multinuclear magnetic resonance structural investigation. *J. Chim. Phys. Phys.-Chim. Biol.* **1998**, *95*, 289–294.

(53) R. A. Sheldon; J. K. Kochi. *Metal-Catalyzed Oxidations of Organic Compounds*; Academic Press: New York, 1981.

(54) R. A. Sheldon. In *Applied Homogeneous Catalysis with Organometallic Compounds*; B. Cornils, W. A. Herrmann, Eds.; Wiley-VCH Verlag GmbH: Weinheim, 2002; Vol. 1: Applications, pp 412–427.

(55) Deubel, D. V.; Sundermeyer, J.; Frenking, G. Mechanism of the Olefin Epoxidation Catalyzed by Molybdenum Diperoxo Complexes: Quantum-Chemical Calculations Give an Answer to a Long-Standing Question. *J. Am. Chem. Soc.* **2000**, *122*, 10101–10108.

(56) Bortolini, O.; Di Furia, F.; Modena, G. Metal Catalysis in Oxidation by Peroxides: Part 171. On the Mechanism of the Vanadium and Molybdenum Catalyzed Oxidation of Sulphides and Olefins Bearing Neighbour Hydroxo Groups by t-Butyl Hydroperoxide and Hydrogen Peroxide. *J. Mol. Catal.* **1983**, *19*, 319–329.

(57) Bhaumik, A.; Tatsumi, T. Selective Dihydroxylation over Titanium Silicate Molecular Sieves. *J. Catal.* **1998**, *176*, 305–309.

(58) Bellussi, G.; Rigutto, M. S. Metal Ions Associated to the Molecular Sieve Framework: Possible Catalytic Oxidation Sites. *Stud. Surf. Sci. Catal.* **1994**, *85*, 177–213.

(59) Mimoun, H.; Postel, M.; Casabianca, F.; Fischer, J.; Mitschler, A. Novel Unusually Stable Peroxotitanium(IV) Compounds. Molecular and Crystal Structure of Peroxobis(picolinato)(Hexamethylphosphoric triamide)Titanium(IV). *Inorg. Chem.* **1982**, *21*, 1303–1306.

(60) Kondo, S.; Saruhashi, K.; Seki, K.; Matsubara, K.; Miyaji, K.; Kubo, T.; Matsumoto, K.; Katsuki, T. A μ-Oxo-μ-η_2:η_2-Peroxo Titanium Complex as a Reservoir of Active Species in Asymmetric Epoxidation Using Hydrogen Peroxide. *Angew. Chem. Int. Ed.* **2008**, *47*, 10195–10198.

(61) Bordiga, S.; Damin, A.; Bonino, F.; Ricchiardi, G.; Lamberti, C.; Zecchina, A. The Structure of the Peroxo Species in the TS-1 Catalyst as Investigated by Resonant Raman Spectroscopy. *Angew. Chem. Int. Ed.* **2002**, *41*, 4734–4737.

(62) Bordiga, S.; Damin, A.; Bonino, F.; Ricchiardi, G.; Zecchina, A.; Tagliapietra, R.; Lamberti, C. Resonance Raman Effects in TS-1: The Structure of Ti(IV) Species and Reactivity towards H_2O, NH_3 and H_2O_2: An in Situ Study. *Phys. Chem. Chem. Phys.* **2003**, *5*, 4390–4393.

(63) Bonino, F.; Damin, A.; Ricchiardi, G.; Ricci, M.; Spanò, G.; D'Aloisio, R.; Zecchina, A.; Lamberti, C.; Prestipino, C.; Bordiga, S. Ti-Peroxo Species in the TS-1/H_2O_2/H_2O System. *J. Phys. Chem. B* **2004**, *108*, 3573–3583.

(64) Bordiga, S.; Groppo, E.; Agostini, G.; van Bokhoven, J. A.; Lamberti, C. Reactivity of Surface Species in Heterogeneous Catalysts Probed by In Situ X-Ray Absorption Techniques. *Chem. Rev.* **2013**, *113*, 1736–1850.

(65) Bregante, D. T.; Flaherty, D. W. Periodic Trends in Olefin Epoxidation over Group IV and V Framework-Substituted Zeolite Catalysts: A Kinetic and Spectroscopic Study. *J. Am. Chem. Soc.* **2017**, *139*, 6888–6898.

(66) Notari, B. Microporous Crystalline Titanium Silicates. *Adv. Catal.* **1996**, *41*, 253–334.

(67) Yoon, C. W.; Hirsekorn, K. F.; Neidig, M. L.; Yang, X.; Tilley, T. D. Mechanism of the Decomposition of Aqueous Hydrogen Peroxide over Heterogeneous TiSBA15 and TS-1 Selective Oxidation Catalysts: Insights from Spectroscopic and Density Functional Theory Studies. *ACS Catal.* **2011**, *1*, 1665–1678.

(68) Bordiga, S.; Bonino, F.; Damin, A.; Lamberti, C. Reactivity of Ti(IV) Species Hosted in TS-1 towards H_2O_2–H_2O Solutions Investigated by Ab Initio Cluster and Periodic Approaches Combined with Experimental XANES and EXAFS Data: A Review and New Highlights. *Phys. Chem. Chem. Phys.* **2007**, *9*, 4854–4878.

(69) Lin, W.; Frei, H. Photochemical and FT-IR Probing of the Active Site of Hydrogen Peroxide in Ti Silicalite Sieve. *J. Am. Chem. Soc.* **2002**, *124*, 9292–9298.

(70) Blackmond, D. G. Reaction Progress Kinetic Analysis: A Powerful Methodology for Mechanistic Studies of Complex Catalytic Reactions. *Angew. Chem., Int. Ed. Engl.* **2005**, *44*, 4302–4320.

(71) Blackmond, D. G. Kinetic Profiling of Catalytic Organic Reactions as a Mechanistic Tool. *J. Am. Chem. Soc.* **2015**, *137*, 10852–10866.

(72) Clerici, M. G.; Bellussi, G.; Romano, U. Synthesis of Propylene Oxide from Propylene and Hydrogen Peroxide Catalyzed by Titanium Silicalite. *J. Catal.* **1991**, *129*, 159–167.

(73) Clerici, M. G.; Ingallina, P. Epoxidation of Lower Olefins with Hydrogen Peroxide and Titanium Silicalite. *J. Catal.* **1993**, *140*, 71–83.

(74) Tourne, C.; Revel, A.; Tourne, G.; Vendrell, M. Heteropolytungstates Containing Elements of the Phosphorus Family with (III) or (V) Oxidation States. Identification of Species X_2W_{19} and XW_9 (X = Phosphorus, Arsenic, Antimony, Bismuth) and Its Relation to XW_{11}. *C R Acad Sci Ser C* **1973**, *277*, 643–645.

(75) Ammari, N.; Herve, G.; Thouvenot, R. A New Class of Organosilyl Derivatives of Polyoxoanions - Attachment of Alkyl-and Arylsilyl Groups on Trivacant Tungstosilicate. *New J. Chem.* **1991**, *15*, 607–608.

(76) Bonhomme, C.; Coelho, C.; Azais, T.; Bonhomme-Coury, L.; Babonneau, F.; Maquet, J.; Thouvenot, R. Some Triple Resonance Experiments in Solid-State CP MAS NMR: V-51/Si-29, P-31/C-13, and Si-29/C-13. *Comptes Rendus Chim.* **2006**, *9*, 466–471.

(77) Zhang, H.; Zhang, Z.; Cui, T.; Lin, Y.-H.; Bhathela, N. A.; Ortega, J.; Worton, D. R.; Goldstein, A. H.; Guenther, A.; Jimenez, J. L.; Gold, A.; Surratt, J. D. Secondary Organic Aerosol Formation via 2-Methyl-3-buten-2-ol Photooxidation: Evidence of Acid-Catalyzed Reactive Uptake of Epoxides. *Environ. Sci. Technol. Lett.* **2014**, *1*, 242–247.

(78) Farrugia, L. J. WinGX Suite for Small-Molecule Single-Crystal Crystallography. *J. Appl. Crystallogr.* **1999**, *32*, 837–838.

(79) Palatinus, L. ; Chapuis, G. SUPERFLIP – A Computer Program for the Solution of Crystal Structures by Charge Flipping in Arbitrary Dimensions. *J. Appl. Crystallogr.* **2007**, *40*, 786–790.

(80) Sheldrick, G. M. Crystal Structure Refinement with SHELXL. *Acta Cryst.* **2015**, C71, 3–8.

Supporting Information

Unveiling the Active Surface Sites in Heterogeneous Titanium-Based Silicalite Epoxidation Catalysts: the Input of Silanol-Functionalized Polyoxotungstates as Soluble Analogues

Teng Zhang,[†] *Louis Mazaud,*[†] *Lise–Marie Chamoreau,*[†] *Céline Paris,*[‡] *Anna Proust*[†] *and Geoffroy Guillemot*[†]*

[†] Sorbonne Université, CNRS, Institut Parisien de Chimie Moléculaire, IPCM, 4 place Jussieu, F-75005 Paris, France.

[‡] Sorbonne Université, CNRS, De la Molécule aux Nano-objets: Réactivité, Interactions et Spectroscopies', MONARIS, 4 place Jussieu, F-75005 Paris, France

geoffroy.guillemot@sorbonne-universite.fr

SECTION 1. STRUCTURAL CHARACTERIZATION OF THE TITANIUM DERIVATIVES

S1.1. Size of the lacuna and metal confinement.

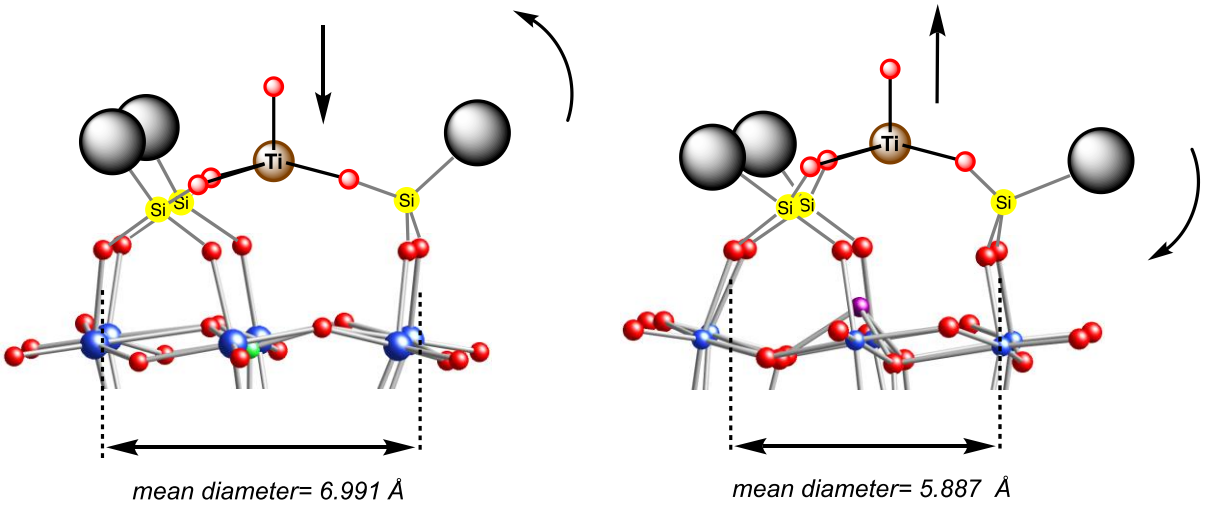

Figure S1. Influence of the size of the lacuna in $[PW_9O_{34}]^{9-}$ (left) and $[SbW_9O_{33}]^{9-}$ (right) on the orientations of the *t*-butyl groups in compounds 3 and 4. The diameter of the lacuna is calculated as the average of the distances that separate opposite oxygen atoms surrounding this lacuna.

Table S1. Crystal data, data collection and structure refinement details.

	THA-3
Crystal data	
Chemical formula	$C_{15}H_{34}O_{38}PSi_3TiW_9 \cdot 3(C_{24}H_{52}N)$
M_r	3704.2
Crystal system, space group	Orthorhombic, *Pbca*
Temperature (K)	120
a, *b*, *c* (Å)	20.2301 (17), 28.431 (2), 43.025 (3)
□, □, □ (°)	90, 90, 90
V (Å^3)	24746(3)
Z	8
Radiation type	Mo *K*□
μ (mm^{-1})	8.503
Crystal size (mm)	0.22 × 0.11 × 0.04
Absorption correction	Multi-scan
θ_{min}, θ_{max}	3.19 , 33.22
No. of measured, independent and observed [$I > 2\sigma(I)$] reflections	432631, 47463, 37485
R_{int}	0.061
$(\sin \theta/\lambda)_{max}$ (Å^{-1})	0.994
$R[F^2 > 2\sigma(F^2)]$, $wR(F^2)$, S	0.0292, 0.0506, 1.064
No. of reflections	47463
No. of parameters	1331
No. of restraints	0
$\Delta\rho_{max}$, $\Delta\rho_{min}$ (e Å^{-3})	1.81, -0.98
CCDC number	1581183

S1.2. Hydrolytic behavior of 3, 4 and 1.

Table S2. Values of the diffusion coefficients measured by DOSY ^{1}H NMR in CD_3CN.

	log(D) [a]	R_H [b] ($\times 10^9$ m)	Volume ratios based on the D values [c]
$[PW_9O_{34}(^tBuSiO)_3Ti(O^iPr)]^{3-}$, **3**	−9.10	0.84	-
$[PW_9O_{34}(^tBuSiO)_3Ti(OH)]^{3-}$, **5**	−9.10	0.84	1
$[SbW_9O_{33}(^tBuSiO)_3Ti(O^iPr)]^{3-}$, **4**	−9.10	0.84	-
$\{[SbW_9O_{33}(^tBuSiO)_3Ti]_2O\}^{6-}$, **6**	−9.29	1.24	3.7

(a) D= diffusion coefficient measured by DOSY ^{1}H NMR experiment (m^2/s)
(b) hydrodynamic radius calculated from the Stokes-Einstein law
(c) from equation (1)

$(V_2/V_1)= (D_1/D_2)^3$ (eq 1)

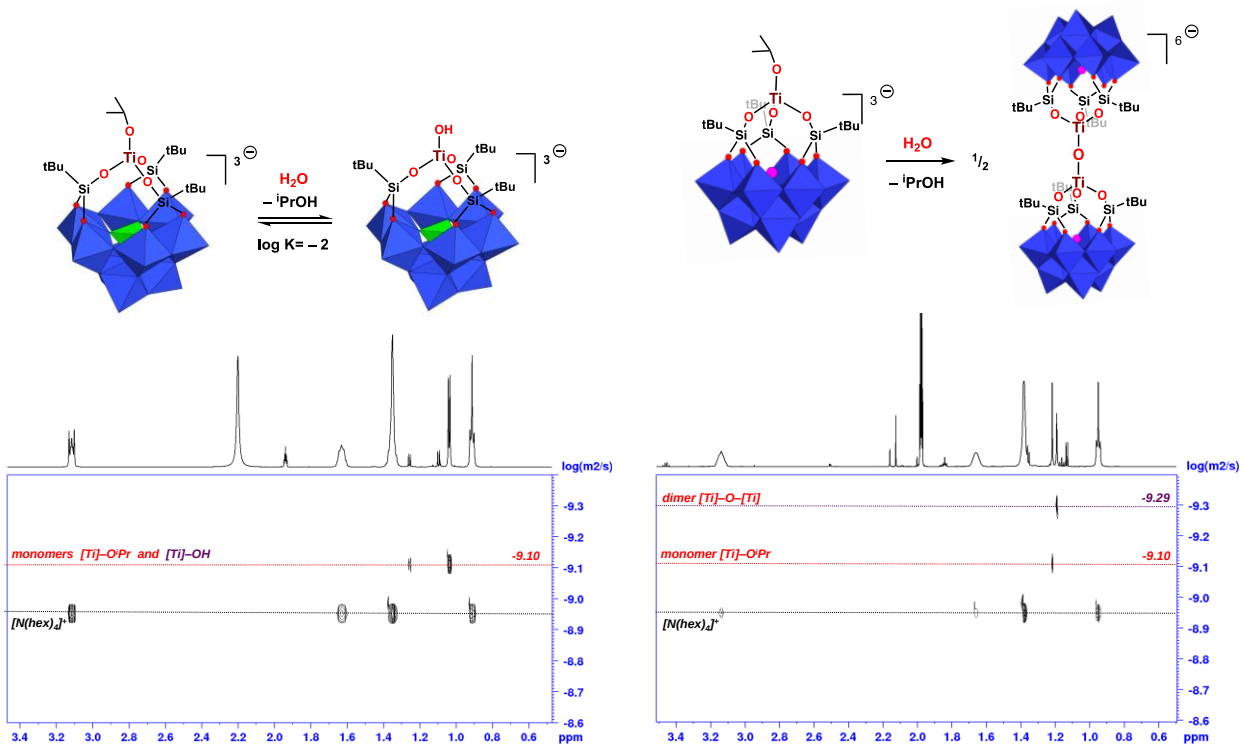

Figure S2. ^{1}H NMR and DOSY NMR of the products of hydrolysis of THA-3 (left) and THA-4 (right).

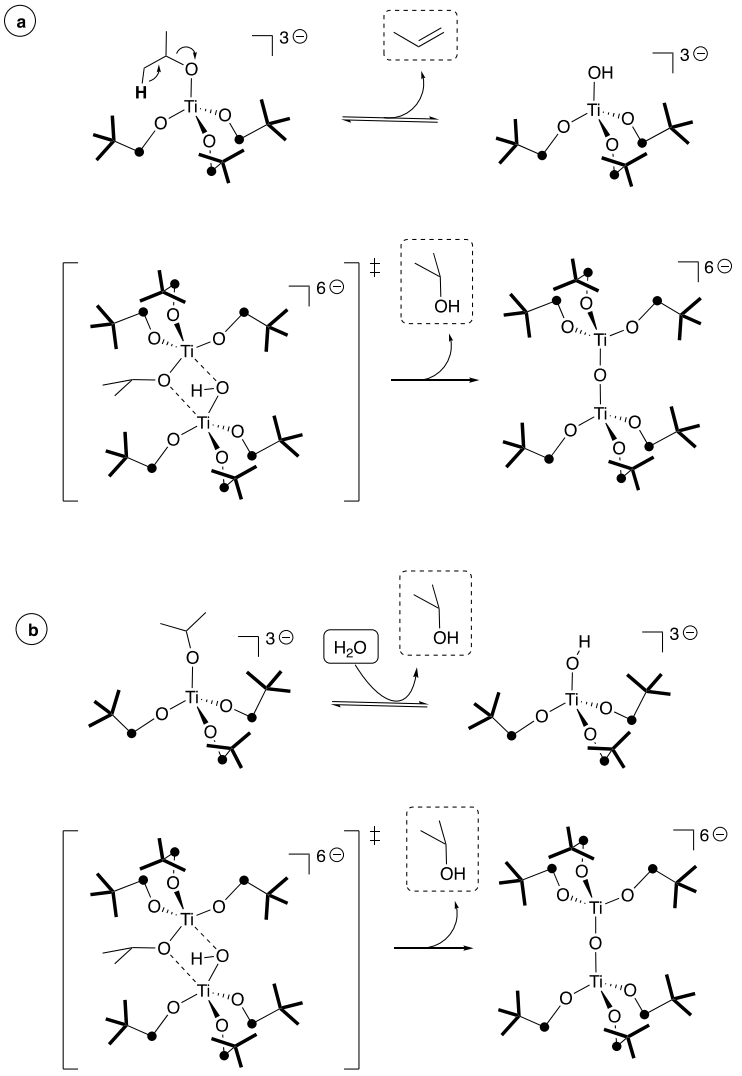

Scheme S1. Two possible pathways for the formation of THA-6 from THA-4: a) via a non-hydrolytic condensation; b) via hydrolysis of the isopropoxide ligand.

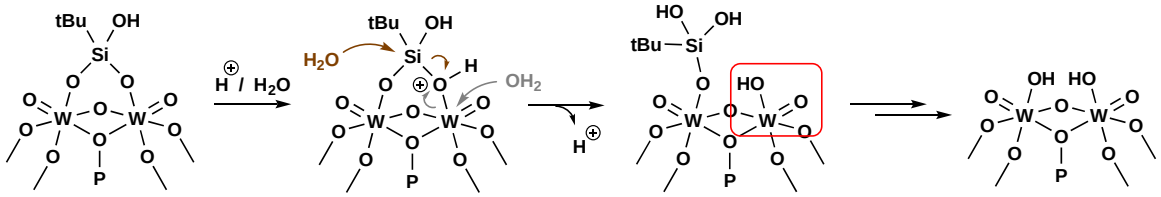

Scheme S2. Proposed pathways for acid-catalyzed hydrolysis of the siloxy functionalities in anion 1: generation of a *cis*-W(=O)(OH) moiety that is the privileged site for the formation of active tungsten-(hydro)peroxide species.

SECTION 2. ACTIVATION OF HYDROGEN PEROXIDE AND CATALYTIC REACTION STUDIES

S2.1. Control experiments: Catalytic activities of [Ti(iOPr)$_4$], THA-1 and THA-2.

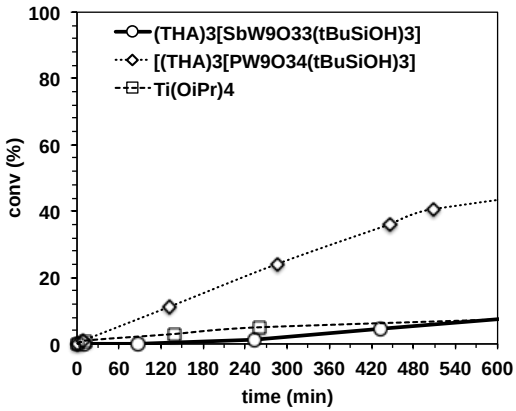

Figure S3. Plot of conversion vs time in the oxidation of 3-methyl-2-buten-1-ol (0.26 M) by H_2O_2 (0.26 M) in CD_3CN at 300 K, catalyzed by 1 mol% of THA-1 (◇), THA-2 (○) or Ti(O^iPr)$_4$ (□).

S2.2. Activation of hydrogen peroxide: NMR studies.

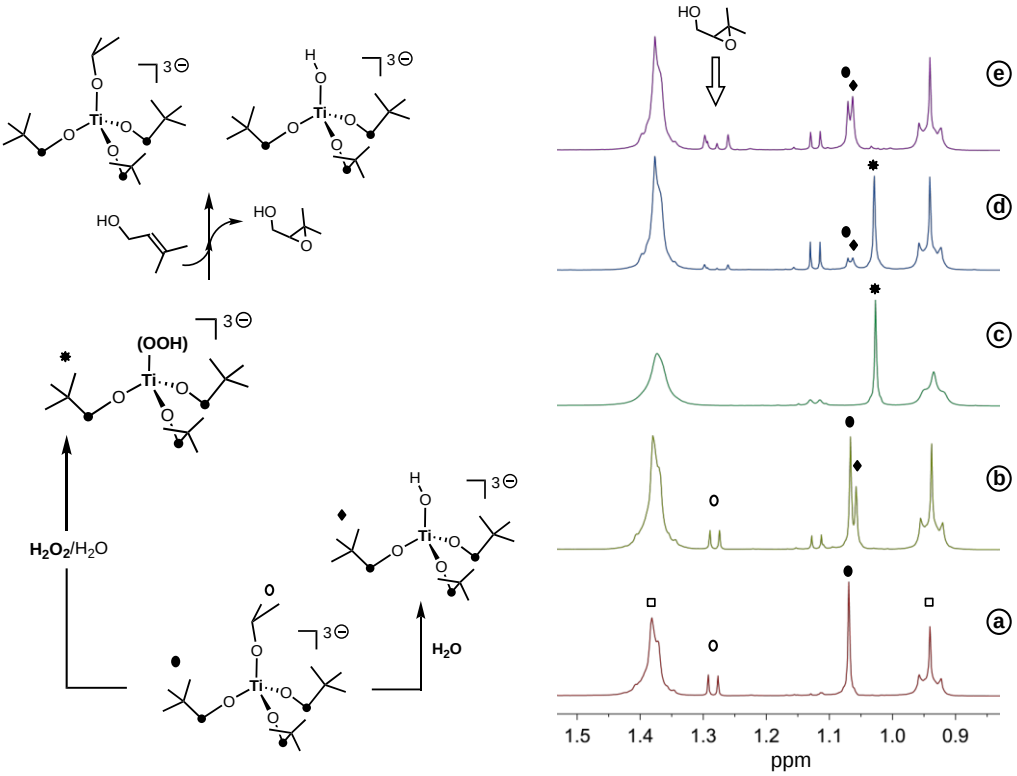

Figure S4. ^{1}H NMR monitoring of the evolution of a 5.2mM solution of (THA)$_3$[PW_9O_{34}(^{t}BuSiO)$_3$Ti(O^iPr)], THA-3, in acetonitrile-d_3 under addition of a aqueous solution of H_2O_2 (30wt%): a) THA-3, peaks reported by a □ mark belong to the tetrahexylammonium cation; b) THA-3 (●) and its product of hydrolysis, THA-5 (♦), formed in the presence of water (50mM); c)

formation of THA-7 after addition of 2 equivalent of H_2O_2 (as a 30wt% aqueous solution) to a) ; d) 8 min. after addition of 2 eq. of 3-methyl-2-buten-1-ol to c) ; e) after 2h of reaction. The doublet at 1.11 ppm belongs to the free 2-propanol.

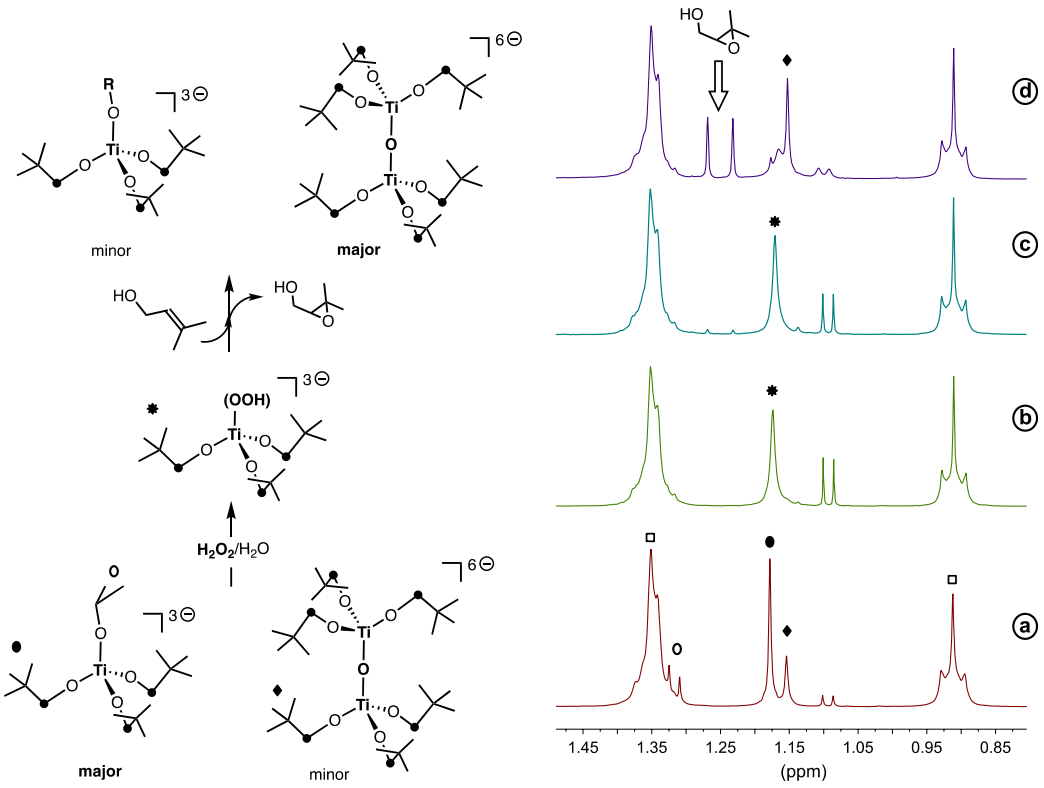

Figure S5. ^{1}H NMR monitoring of the evolution of a 5.2mM solution of $(THA)_3[SbW_9O_{33}(^tBuSiO)_3Ti(O^iPr)]$, THA-4, in acetonitrile-d_3 under addition of a aqueous solution of H_2O_2 (30wt%): a) THA-4 (●, major) and the related dimer, THA-6 (♦, minor); peaks reported by a □ mark belong to the tetrahexylammonium cation; b) formation of THA-8 after addition of 2 equivalent of H_2O_2 (as a 30wt% aqueous solution) to a) ; c) 8 min. after addition of 3 eq. of 3-methyl-2-buten-1-ol to b) ; d) after 2h of reaction. The doublet at 1.11 ppm belongs to the free 2-propanol.

S2.3. Activation of hydrogen peroxide: UV-Vis studies.

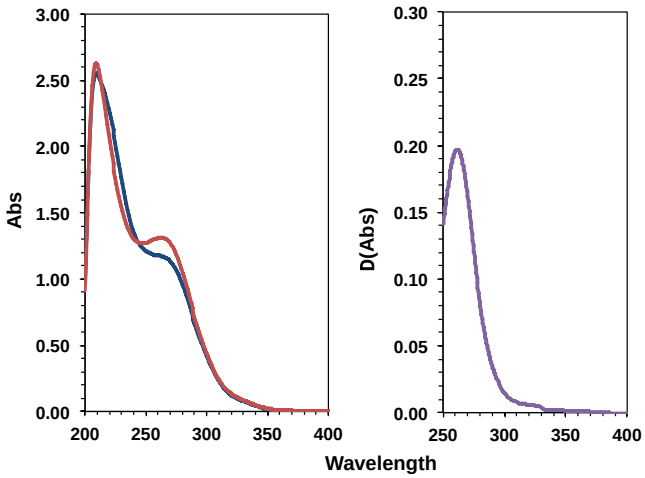

Figure S6. Left: UV-Vis spectra of $(THA)_3[SbW_9O_{33}(^tBuSiO)_3Ti(O^iPr)]$ (THA-4) in acetonitrile (blue line) and after addition of aqueous hydrogen peroxide (red line); (right) result of the subtraction of UV-vis spectra.

S2.4. Catalytic Olefin Epoxidation: Kinetic Studies.

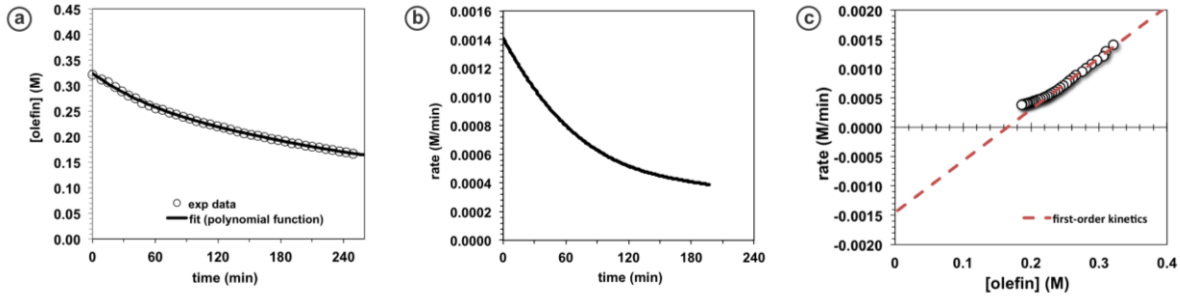

Figure S7. Kinetic profiles from reaction of Table 3, Entry 3. (a) [3-Me-2-buten-1-ol] vs time and the corresponding fit using a fifth order polynomial function; (b) Differentiation of the polynomial function allow to plot the rate vs time ; (c) rate vs [3–methyl–2–buten–1–ol]. The linear behavior with non zero intercept related to value of [xs] indicates a first-order in $[H_2O_2]$ and a zero-order in [3-Me-2-buten-1-ol] as detailed below.

$[H_2O_2]$ = [olefin] – [xs]
rate = $k\cdot[H_2O_2]$ = $k\cdot$[olefin] – $k\cdot$[xs]
Equation from Figure S7c gives : f(x) = a·x + b = 8.7908 10^{-3} x – 1.4523 10^{-3}
Slope = $\boldsymbol{k}$ = **8.79 10^{-3} min^{-1}**
At y intercept: **f(0) = –1.45 mM/min**, which is in good agreement with calculated – $\boldsymbol{k}\cdot$**[xs] = –1.32 mM/min**